TKK Radio Science and Engineering Publications
Espoo 2009 REPORT R11

ARTIFICIAL IMPEDANCE SURFACES

Thesis for the degree of Doctor of Science in Technology

Olli Luukkonen

Dissertation for the degree of Doctor of Science in Technology to be presented with due permission of the Faculty of Electronics, Communications and Automation, for public examination and debate in Auditorium S 4 at Helsinki University of Technology (Espoo, Finland) on the 14th of December, 2009, at 10 a.m.

Helsinki University of Technology
Faculty of Electronics, Communications and Automation
Department of Radio Science and Engineering

Distribution:
Helsinki University of Technology
Department of Radio Science and Engineering
P.O. Box 3000
FI-02015 TKK
Tel. +358 9 470 22261
Fax +358 9 470 22267
E-mail: ari.sihvola@tkk.fi

ISBN 978-952-248-251-8 (paper)
ISBN 978-952-248-252-5 (electronic)
ISSN 1797-4364 (paper)
ISSN 1797-8467 (electronic)

Picaset Oy
Helsinki 2009

ABSTRACT OF DOCTORAL DISSERTATION	HELSINKI UNIVERSITY OF TECHNOLOGY P. O. BOX 1000, FI-02015 TKK http://www.tkk.fi

Author Olli Luukkonen

Name of the dissertation
Artificial impedance surfaces

Manuscript submitted July 17, 2009	Manuscript revised November 4, 2009
Date of the defence December 14, 2009	
☐ Monograph	☒ Article dissertation (summary + original articles)

Faculty	Electronics, Communications and Automation
Department	Radio Science and Engineering
Field of research	Radio Engineering, Electromagnetics
Opponent(s)	Professor Stefano Maci, University of Siena
Supervisor	Professors Antti Räisänen and Sergei Tretyakov
Instructor	Professor Sergei Tretyakov

Abstract

In this doctoral thesis the properties of certain artificial impedance surfaces and electromagnetic materials are studied. In the context of the thesis the word artificial refers to the electromagnetic properties of homogeneous surfaces and materials, that are not naturally observed in nature. The macroscopic electromagnetic properties of these homogeneous materials are determined by their microscopic structures. Therefore it is convenient to call these surfaces and materials also as metasurfaces and metamaterials, which are the common names in the literature for the surfaces and materials studied in this doctoral thesis. This work concentrates on the analytical modeling and applications of such structures.

The purpose of the analytical models of artificial impedance surfaces is to understand the physical properties of the structures and to facilitate the use of these structures in different applications. Sometimes the information given by the analytical models leads to innovations and new findings. For the artificial impedance surfaces studied in this doctoral thesis there have been no accurate and physically exact models available in the literature. In this work we have derived analytical models for various artificial surfaces and verified them to be accurate by numerical and experimental methods. We have used these models in the thesis work to study the properties of these surfaces. Further, we have used the derived analytical models to design different applications based on the artificial impedance surfaces. I have also been able to show the existence of previously unknown plasmonic resonance in electrically thin artificial impedance surface structures.

The results of this doctoral thesis bring more insight into the properties of artificial impedance surfaces. These results are important when designing novel impedance surfaces and applications based on these surfaces.

Keywords	Artificial impedance surface, electromagnetic materials		
ISBN (printed)	978-952-248-251-8	ISSN (printed)	1797-4364
ISBN (pdf)	978-952-248-252-5	ISSN (pdf)	1797-8467
Language	English	Number of pages	82 + appendix 74
Publisher	Helsinki University of Technology, Department of Radio Science and Engineering		
Print distribution	Helsinki University of Technology, Department of Radio Science and Engineering		

☒ The dissertation can be read at http://lib.tkk.fi/Diss2009/

VÄITÖSKIRJAN TIIVISTELMÄ	TEKNILLINEN KORKEAKOULU PL 1000, 02015 TKK http://www.tkk.fi

Tekijä Olli Luukkonen

Väitöskirjan nimi
Keinotekoiset impedanssipinnat

Käsikirjoituksen päivämäärä 17.7.2009	Korjatun käsikirjoituksen päivämäärä 04.11.2009
Väitöstilaisuuden ajankohta 14.12.2009	
☐ Monografia	☒ Yhdistelmäväitöskirja (yhteenveto + erillisartikkelit)

Tiedekunta	Elektroniikan, tietoliikenteen ja automaation tiedekunta
Laitos	Radiotieteen ja -tekniikan laitos
Tutkimusala	Radiotekniikka, sähkämagnetiikka
Vastaväittäjä(t)	Professori Stefano Maci, University of Siena
Työn valvoja	Professorit Antti Räisänen ja Sergei Tretyakov
Työn ohjaaja	Professori Sergei Tretyakov

Tiivistelmä

Tässä väitöskirjassa tutkitaan tiettyjä keinotekoisia impedanssipintoja ja sähkömagneettisia materiaaleja. Väitöskirjatyön kontekstissa keinotekoisuudella tarkoitetaan pintojen tai materiaalien sähkömagneettisia ominaisuuksia, joita ei tavata luonnossa tavallisesti. Näiden materiaalien makroskooppiset sähkömagneettiset ominaisuudet syntyvät niiden mikroskooppisista rakenteista. Täten onkin sopivaa nimittää kyseisiä pintoja ja materiaaleja myös nk. metapinnoiksi ja -materiaaleiksi, millä nimillä väitöskirjassa käsiteltyjä pintoja ja materiaaleja tavallisesti kirjallisuudessa kutsutaankin. Tässä työssä keskitymme kyseisten rakenteiden analyyttiseen mallintamiseen ja niihin liittyviin sovelluksiin.

Keinotekoisten impedanssipintojen analyyttisten mallien tarkoitus on ymmärtää rakenteiden fysikaalisia ominaisuuksia ja helpottaa niiden käyttämistä erilaisissa sovelluksissa. Joskus analyyttisten mallien tuoma tieto rakenteiden fysikaalisista ominaisuuksista johtaa uusiin innovaatioihin tai löydöksiin. Tässä väitöskirjassa tutkituille keinotekoisille impedanssipinnoille ei aikaisemmin ole ollut kirjallisuudessa tarkkoja ja fysikaalisesti eksakteja malleja tarjolla. Tässä työssä olemme johtaneet kyseisille pinnoille analyyttisiä malleja ja olemme osoittaneet ne myös tarkoiksi numeerisin ja kokeellisin menetelmin. Olemme käyttäneet näitä malleja tässä työssä kyseisten pintojen ominaisuuksien tutkimiseen. Lisäksi olemme käyttäneet johdettuja analyyttisiä malleja erilaisten keinotekoisiin impedanssipintoihin perustuvien sovellusten suunnittelemiseen. Olemme myös pystyneet osoittamaan aikaisemmin tuntemattoman plasmonisen resonanssin olemassa olon sähköisesti ohuissa keinotekoisissa impedanssipinta rakenteissa.

Tämän väitöskirjan tulokset tuovat lisää ymmärrystä keinotekoisten impedanssipintojen ominaisuuksista. Nämä tulokset ovat tärkeitä suunniteltaessa uusia impedanssipintoja ja kyseisiin pintoihin perustuvia sovelluksia.

Asiasanat keinotekoiset impedanssipinnat, sähkämagneettiset materiaalit

ISBN (painettu) 978-952-248-251-8	ISSN (painettu) 1797-4364
ISBN (pdf) 978-952-248-252-5	ISSN (pdf) 1797-8467
Kieli Englanti	Sivumäärä 82 + liitteet 74

Julkaisija Teknillinen korkeakoulu, Radiotieteen ja -tekniikan laitos

Painetun väitöskirjan jakelu Teknillinen korkeakoulu, Radiotieteen ja -tekniikan laitos

☒ Luettavissa verkossa osoitteessa http://lib.tkk.fi/Diss2009/

Preface

This thesis summarizes selected results obtained in the Department of Radio Science and Engineering (former Radio Laboratory) of TKK Helsinki University of Technology under the supervision of Professors Sergei Tretyakov and Antti Räisänen. I want to thank my supervisors for the opportunity to be able to work on this interesting topic for my thesis.

Especially, I want to express my gratitude to Professor Sergei Tretyakov for being able to work in a highly recognized research group for all these years. Your guidance together with Professor Constantin Simovski has been excellent. The stimulating discussion I have had with you two during these years and your teachings have shaped my understanding and thinking of electromagnetics and radio science.

I thank Professors Igor Nefedov, Alexander Yakovlev, Gérard Granet, and Agostino Monorchio as well as Dr Mário Silveirinha, Dr George Goussetis, Dr Dmitri Lioubtchenko, Mr Pekka Alitalo, and Mr Filippo Costa for your help and important input in the studies on analytical modeling of artificial impedance surfaces. I have enjoyed working with you and our numerous discussions on the topic. It has been a privilege to work with you.

I wish to thank also the present and former personnel of the Department of Radio Science and Engineering and Radio Laboratory for the past immemorial years.

I am thankful for the pre-examiners Dr Alexandros Feresidis and Dr Christopher Holloway for reviewing the manuscript and for the valuable comments and advises regarding it.

During my studied I have received financial support from Jenny ja Antti Wihurin Rahasto, Elektroniikkainsinöörien Seura, Emil Aaltosen Säätiö, Nokia Foundation, Fulbright, and Tekniikan Edistämissäätiö. This support is gratefully acknowledged.

I am thankful to my parents Pirjo and Risto Luukkonen, and to my sisters Hanna, Eeva, and Liisa for the encouragement during the whole course of my studies.

Finally, my dearest thanks are to Satu for your support throughout my studies and research.

Otaniemi, November 4, 2009, Olli Luukkonen

Contents

List of Publications

This thesis consists of an overview and of the following publications which are referred to in the text by Roman numerals.

I **O. Luukkonen**, C. Simovski, G. Granet, G. Goussetis, D. Lioubtchenko, A. V. Räisänen, and S. A. Tretyakov, "Simple and accurate analytical model of planar grids and high-impedance surfaces comprising metal strips or patches," *IEEE Transactions on Antennas and Propagation*, vol. 56, no. 6, pp. 1624–1632, 2008.

II **O. Luukkonen**, C. Simovski, A. V. Räisänen, and S. A. Tretyakov, "An efficient and simple analytical model for analysis of propagation properties in impedance waveguides," *IEEE Transactions on Microwave Theory and Techniques*, vol. 56, no. 7, pp. 1624–1632, 2008.

III **O. Luukkonen**, M. G. Silveirinha, A. B. Yakovlev, C. R. Simovski, I. S. Nefedov, and S. A. Tretyakov, "Effects of spatial dispersion on reflection from mushroom-type artificial impedance surfaces," *IEEE Transactions on Microwave Theory and Techniques*, vol. 57, no. 11, pp. 2692–2699, Nov. 2009.

IV **O. Luukkonen**, C. R. Simovski, and S. A. Tretyakov, "Grounded uniaxial material slabs as magnetic conductors," *Progress in Electromagnetic Research B*, vol. 15, pp. 267–283, 2009.

V **O. Luukkonen**, P. Alitalo, C. R. Simovski and S. A. Tretyakov, "Experimental verification of an analytical model for high-impedance surfaces," *Electronics Letters*, vol. 45, no. 14, pp. 720–721, 2009.

VI **O. Luukkonen**, F. Costa, C. R. Simovski, A. Monorchio, and S. A. Tretyakov, "A thin electromagnetic absorber for wide incidence angles and both polarizations," *IEEE Transactions on Antennas and Propagation*, vol. 57, no. 10, pp. 3119–3125, Oct. 2009.

VII **O. Luukkonen**, A. B. Yakovlev, C. Simovski, and S. A. Tretyakov, "Comparative study of surface waves on high-impedance surfaces with and without vias," *Proc. 2008 IEEE AP-S International Symposium on Antennas and Propagation, San Diego*, paper s326p3, July 5–12, 2008.

Author's contribution

All papers [**I**] - [**VI**] are mainly written by the author of this thesis. More detailed contributions are indicated below.

In [**I**] the idea for the paper was formulated by the author together with the co-authors. The analytical derivations were conducted together with Professor Constantin Simovski and Professor Sergei Tretyakov. The numerical simulations were done by the author together with Professor Gérard Granet and Dr George Goussetis.

In [**II**] the author developed the theory section together with Professor Constantin Simovski and Professor Sergei Tretyakov. The numerical simulations were done by the author.

In [**III**] the idea for the paper was formulated by the author together with all the co-authors. The analytical derivations and the numerical simulations were all done by the author together with Dr Mário Silveirinha.

In [**IV**] the analytical derivations and numerical simulations were conducted by the author.

In [**V**] the measurements were conducted by the author together with Mr Pekka Alitalo. The simulations were conducted by the author.

In [**VI**] the idea of the paper was formulated by the author and the analytical derivations were conducted also by the author. The numerical simulations were conducted by the author together with Mr Filippo Costa.

In [**VII**] the author developed the theory section together with Professor Constantin Simovski and Professor Sergei Tretyakov. The numerical simulations were done by the author.

In addition to the above publications the author has authored and co-authored publications [1]- [11] related to the topic of this thesis.

List of Abbreviations

TE	Transverse Electric
TM	Transverse Magnetic
HFSS	High-Frequency Structure Simulator
MEMS	Microelectromechanical System
EBG	Electromagnetic band-gap
PBG	Photonic band-gap
PEC	Perfect Electric Conductor

List of Symbols

a, b	Periodicity or lattice constant
$C_{\mathrm{g}}^{\mathrm{TM}}$	Averaged effective capacitance of a grid for TM fields
$C_{\mathrm{g}}^{\mathrm{TE}}$	Averaged effective capacitance of a grid for TE fields
C_{var}	Varactor capacitance
$\mathbf{D}$	Electric flux density vector
$E_{\mathrm{x}}^{\mathrm{loc}}$	Local x-directed electric field
$E_{\mathrm{x}}^{\mathrm{w}}$	Electric field created by the wire along the x-axis
$E_{\mathrm{x}}^{\mathrm{ext}}$	External x-directed electric field
$\mathbf{E}_{\mathrm{t}}$	Transverse component of the electric field
$\mathbf{E}_{\mathrm{t}+}$	Transverse component of the electric field at the upper surface
$\mathbf{H}_{\mathrm{t}}$	Transverse component of the magnetic field
$\mathbf{H}_{\mathrm{t}+}$	Transverse component of the magnetic field at the upper surface
h	Height of the substrate
I	Electric current
$\overline{\overline{I}}_{\mathrm{t}}$	Transverse unit dyadic
j	Imaginary unit
k	Wave number
k_0	Wave number in free space
k_{eff}	Effective wave number
k_{p}	Plasma wave number
k_{t}	Transverse wave number
k_{x}	Wave number along the x-axis
k_{y}	Wave number in the y-direction
k_{z}	Propagation constant along the normal direction in free space (along the z-axis)
$\mathbf{k}_{\mathrm{t}}$	Transverse component of the wave vector
$\mathbf{n}$	Unit vector along the normal of a surface
r_0	Radius of a wire
w	Width of a strip or a gap
$\mathbf{x}_0$	Unit vector along the x-direction
$\mathbf{y}_0$	Unit vector along the y-direction
Z	Impedance
Z_{d}	Surface impedance of a grounded dielectric slab
$Z_{\mathrm{g}}^{\mathrm{TM}}$	Grid impedance for TM fields
$Z_{\mathrm{g}}^{\mathrm{TE}}$	Grid impedance for TE fields
Z_{inp}^{+}	Surface impedance of the upper waveguide wall
Z_{inp}^{-}	Surface impedance of the lower waveguide wall
Z_{s}	Surface impedance
Z_0^{TE}	Free-space impedance of TE fields
Z_0^{TM}	Free-space impedance for TM fields

α_{TM}	Grid parameter for the TM fields
α_{TE}	Grid parameter for the TE fields
β	Wave number in the normal direction in a material slab
β_{TM}	Propagation constant along the normal for TM fields
β_{TE}	Propagation constant along the normal for TE fields
γ_{TM}	Propagation constant along the normal direction for TM polarization in wire medium
Δ	Correction factor
ε	Permittivity
$\varepsilon_{\mathrm{eff}}$	Relative effective permittivity
ε_1	Relative permittivity of medium 1
ε_2	Relative permittivity of medium 2
$\varepsilon_{\mathrm{n}}^{\mathrm{TM}}$	Relative effective permittivity along the wires in wire medium
ε_{n}	Permittivity along the normal direction
ε_{t}	Permittivity along the transverse direction
η	Wave impedance
η_0	Wave impedance in free space
η_{eff}	Effective wave impedance
θ	Angle of incidence
θ_2	Angle of refraction
λ	Wavelength
μ	Permeability
μ_{n}	Permeability along the normal direction
μ_{t}	Permeability along the transverse direction
ω	Angular frequency
∇_{t}	Transverse nabla

List of Figures

1 Introduction

The electromagnetic properties of homogeneous materials arise from the microstructure and chemical composition of the material. These properties, generally measured by permittivity and permeability, dictate the response of the material to external electric and magnetic fields, respectively. In artificial electromagnetic materials the microstructure of the material is man-made and, in general, designed for a particular function or application. In artificial microstructures, the electromagnetic properties that these materials posses are often not readily found in nature. Also, the dimensions of the building blocks or particles are electrically small, that is, the overall size of the building block is much smaller than the wavelength of the electromagnetic wave. Therefore it is convenient to refer to these materials also as metamaterials, which is a common name for this type of materials in the literature. Compared to the artificial electromagnetic materials, in artificial impedance surfaces the structure is bound into two dimensions. This doctoral thesis concentrates on such artificial impedance surfaces.

In electromagnetic theory it is convenient to model surfaces with boundary conditions where the surface impedance of a structure denotes the ratio of the tangential electric and magnetic field components on that surface. This type of closed-form expressions for the electromagnetic properties or analytical models of the artificial impedance surfaces is extremely useful when studying the properties of various types of surfaces and especially when designing applications where the artificial impedance surface is just one of the building blocks of a larger system. Further, these analytical models bring physical insight and provide information about the artificial impedance surface that can lead to innovations and new applications. For the artificial impedance surfaces studied in this doctoral thesis there have been no accurate and physically sound models available in the literature.

In this doctoral thesis the properties of different types of artificial impedance surfaces are studied. The main emphasis of the work is on the analytical modeling of artificial impedance surfaces. In addition, the properties of the studied surfaces are applied to electromagnetic absorbers, impedance waveguides, and electromagnetic band gap structures for antenna applications. The objectives of this work are to find accurate closed-form expressions for the electromagnetic fields on the surface of the studied artificial impedance structure that would model the properties of the surface in a physically correct manner. Further, to use the insight given by these analytical models to design applications based on the exotic properties of these surfaces.

The research methods used in this doctoral thesis include derivation of analytical expressions for the properties of the artificial impedance surfaces and their applications as well as numerical verification of the predicted results. In addition, the results in some cases have been verified experimentally and compared to other results available in the literature.

The rest of the thesis is organized in the following manner:

Chapter 2 discusses very generally the use of impedance boundary conditions in electro-

magnetics with a view to familiarize the reader with this subject, which is closely related to the topic of this thesis.

In Chapter 3 and paper [**I**] the properties of capacitive screens are studied. The properties of these screens are essential for the operation of the artificial impedance surfaces and therefore their correct and accurate analytical modeling is crucial for the future work of modeling of artificial impedance surfaces. Example results are shown and comparison with other results available in the literature is done.

In Chapter 4 and papers [**I-V**] the properties of different types of artificial surfaces are studied. The studied artificial impedance surfaces are composed of a capacitive grid over a grounded dielectric slab. The grounded dielectric slab can be perforated with vertical metallic vias connecting the grid or mesh on the substrate to the ground plane or there can be no vias; both cases are considered. The differences of these two types of surfaces for surfaces waves are also studied. Furthermore, a plasmonic resonance found in the artificial impedance surfaces structures and its connection to novel boundary conditions is discussed. The scientific contributions of this chapter include accurate analytical models for different artificial impedance surfaces and study of the propagation properties of surface waves on some of the studied surfaces.

In Chapter 5 and papers [**II**,**VI**,**VII**] some applications based on the artificial impedance surfaces discussed in the previous chapter are studied. The considered applications are electromagnetic absorbers [**VI**], tunable impedance waveguides [**II**], and electromagnetic band gap structures [**VII**]. The design of the electromagnetic absorbers is based on the artificial impedance surfaces studied in the previous chapter. In this chapter the possibility to use the plasmonic resonance for enlarging the absorption band of the absorber is studied. In the case of tunable impedance waveguides, the propagation properties of parallel-plate waveguides are studied when the sidewalls of the waveguides have been replaced with one or two tunable artificial impedance surfaces. The scientific contributions of this chapter include novel methods to improve the performance of these devices as well as accurate analytical models for these applications.

Contributions of the original publications are provided at the end of the corresponding chapters and the conclusions of the thesis as well as the summary of the contributions are given in Chapter 6.

2 Averaged boundary conditions in general

The possibility to simplify solutions of electromagnetic problems is one of the main motivations of this thesis. Especially, in the case of complicated artificial impedance surfaces that are parts of a bigger system, an accurate approximative boundary condition eases the analysis of the system considerably. While imposing a boundary condition, the fields behind the boundary have been calculated and their response at the boundary is known. The purpose is not to find an exact field distribution at the boundary but rather a smoothly varying averaged distribution that would create the same fields as the exact distribution at some distance away from the boundary. It is then possible to replace the complicated structure with a boundary condition that connects the tangential electric and magnetic fields. Therefore these boundary condition are referred as impedance or transition conditions. After imposing the boundary condition, the fields behind the boundary have no physical meaning. In the following a boundary condition for an interface with an isotropic material is derived and the different orders of approximations for this condition are explained more thoroughly. Finally, the principles of the derivation of the boundary condition for the inductive grids considered in the forthcoming parts of this thesis are explained in general. Many books have been written on this topic and an interested reader is directed to [12–14]. The following discussion will generally follow the treatment of impedance boundary conditions as done by Tretyakov [14].

Let us consider a semi-infinite isotropic material with permittivity ε and permeability μ having an interface at $z = 0$. It is possible to find an exact boundary condition for the tangential fields at this interface in the Fourier domain (for plane waves) and in the physical domain. However, in the physical domain the operational boundary conditions require always certain degree of approximations, as shall be seen later. In the following the exact boundary condition for the case of semi-infinite material sample is written in the Fourier domain. The boundary condition for the physical domain can then be easily derived from here.

From Maxwell's equations we find that the tangential fields with respect to the material interface in the isotropic material can be written as

$$\frac{\partial}{\partial z}\mathbf{n} \times \mathbf{E}_{\mathrm{t}} = -j\omega\mu\mathbf{H}_{\mathrm{t}} - \frac{1}{j\omega\varepsilon}\nabla_{\mathrm{t}} \times (\nabla_{\mathrm{t}} \times \mathbf{H}_{\mathrm{t}}), \tag{2.1}$$

where

$$\mathbf{E}_{\mathrm{t}} \cdot \mathbf{n} = 0, \quad \mathbf{H}_{\mathrm{t}} \cdot \mathbf{n} = 0, \quad \nabla_{\mathrm{t}} = \frac{\partial}{\partial x}\mathbf{x}_0 + \frac{\partial}{\partial y}\mathbf{y}_0 \tag{2.2}$$

and $\mathbf{n} = \mathbf{z}_0$ is the normal of the surface. For simplicity, let us consider only the case for the TM-polarized fields. In this case the magnetic field has only a component along the x-axis (H_{x}) and the electric fields has components along both y- and z-axes (E_{y} and E_{z}, respectively). For this polarization only the magnetic field component H_{x} and the electric field component E_{y} enter equation (2.1). In this case (2.1) simplifies to (omitting

the $e^{-jk_y y}e^{j\beta z}$ dependency of the fields):

$$\frac{\partial}{\partial z}E_{\mathrm{y}} = \left(j\omega\mu + \frac{k_{\mathrm{y}}^2}{j\omega\varepsilon}\right)H_{\mathrm{x}}. \tag{2.3}$$

We can integrate (2.3) over the material volume from the minus infinity to zero and get rid of the derivative on the left side. This would correspond to averaging of the fields over the whole material thickness. Assuming that the material has some losses, the fields very far away from the interface disappear, and (2.1) can be written as

$$E_{\mathrm{y}+} = \left(j\omega\mu + \frac{k_{\mathrm{y}}^2}{j\omega\varepsilon}\right)\cdot\int_{-\infty}^{0} H_{\mathrm{x}}dz, \tag{2.4}$$

where $+$ refers to the surface of the interface. In the material ($z < 0$), the general solution for the tangential magnetic fields read

$$H_{\mathrm{x}} = H_{\mathrm{x}+}e^{j\beta z}, \tag{2.5}$$

where $\beta = \sqrt{k^2 - k_{\mathrm{y}}^2}$ ($\mathrm{Im}\,(\beta) < 0$) is the wave number in the normal direction in the material, $k = \omega\sqrt{\varepsilon\mu}$ is the wave number in the material, and k_{y} is the wave number in the y-direction (in this case also the transverse wave number). The integral of the tangential magnetic fields in (2.4) gives

$$\int_{-\infty}^{0} H_{\mathrm{x}}dz = \frac{1}{j\beta}H_{\mathrm{x}+}. \tag{2.6}$$

We can now rewrite (2.4) as

$$E_{\mathrm{x}+} = \eta\sqrt{1 - \frac{k_{\mathrm{y}}^2}{k^2}}H_{\mathrm{x}+}, \tag{2.7}$$

where $\eta = \sqrt{\frac{\mu}{\varepsilon}}$ is the wave impedance. This is the exact boundary condition for a semi-infinite isotropic material in the Fourier domain. We can transfer this to the physical domain by replacing the tangential wave numbers with differential tangential operators ($k_{\mathrm{y}} \to j\frac{\partial}{\partial y}$)

$$E_{\mathrm{y}+} = \eta\sqrt{1 + \frac{1}{k^2}\frac{\partial^2}{\partial y^2}}H_{\mathrm{x}+}. \tag{2.8}$$

This, however, is not practically useful boundary condition because of the pseudodifferential operator $\sqrt{1 + \frac{1}{k^2}\frac{\partial^2}{\partial y^2}}$. In practice certain approximations are needed for the pseudodifferential operator in order to get a functional boundary condition. For instance, one can expand the operator into the Taylor series and choose an appropriate approximation. This brings us to the discussion on the accuracy and the order of the boundary conditions.

Let us first define the order of the boundary conditions considered in this thesis to be that of the highest order of the tangential derivatives included in the boundary condition. We can expand the pseudodifferential operator into the Taylor series as

$$\sqrt{1 + \frac{1}{k^2}\frac{\partial^2}{\partial y^2}} = \left(1 + \frac{1}{2k^2}\frac{\partial^2}{\partial y^2} - \frac{1}{8k^4}\frac{\partial^4}{\partial y^4} + \frac{1}{16k^6}\frac{\partial^6}{\partial y^6} + \ldots\right) \tag{2.9}$$

where the first four terms of the approximation are written. By including the first two, three, or four terms into the approximation we respectively get the second-, fourth-, and sixth-order boundary conditions. For an exact boundary conditions in the physical domain all the spatial derivatives would be needed. Naturally, also other approximations for the pseudodifferential operator can be used. The choice of the approximation (and its order) depends largely on the application and the required accuracy.

So far we have derived a boundary condition for a simple example. In principle, many boundary conditions can be derived in a similar manner; first we need to find averaged tangential fields on the surface and then connect them to one another. Let us consider an inductive grid comprising thin electrically conductive wires along the x-axis, for instance. In order to derive a boundary condition for this structure we first need to calculate the fields at a certain wire of the grid to find out the induced current on that wire. To do this, we sum up the exciting external field at this point together with the field components created by all the wires in the system excited by this same external field:

$$E_{\mathrm{x}}^{\mathrm{loc}} + E_{\mathrm{x}}^{\mathrm{w}} + E_{\mathrm{x}}^{\mathrm{ext}} = ZIe^{-jk_{\mathrm{x}}x}, \tag{2.10}$$

where $E_{\mathrm{x}}^{\mathrm{loc}}$ is the local electric field along the x-axis created by all the other wires in the grid, $E_{\mathrm{x}}^{\mathrm{w}}$ is the field created by the wire itself, $E_{\mathrm{x}}^{\mathrm{ext}}$ is the exciting external field, Z is the impedance per unit length of the wire, I is the current on the wire, and k_{x} is the wave number in the x-direction. We can then average the current over the grid and connect the averaged current to the averaged tangential fields scattered by the grid. By summing up the scattered and incident fields at the grid we can derive a relation between the averaged total fields on the grid and hence our boundary condition.

In what follows, averaged boundary conditions, such as the ones derived in this section, are studied for particular capacitive screens. First, literature is reviewed for the work done on analytical modeling of inductive and capacitive screens. The literature review is limited to screens composed of periodically organized grids of parallel strips or wires referred to as *inductive* or *capacitive grids*, and to *inductive* or *capacitive meshes*. In inductive and capacitive meshes the strips on a plane are organized in two orthogonal directions and bonded to one another at intersections.

3 Analytical modeling of capacitive grids and meshes

3.1 Introduction

In the simplest artificial impedance surface a capacitive grid is positioned over a grounded dielectric slab in order to create a resonant structure. No metallic inclusions are embedded in the dielectric substrate, as in mushroom-type impedance surfaces. The capacitive grid can be an array of square patches in order to have an isotropic response from the surface, but the grid can also be anisotropic and comprise rectangular patches or strips. The correct and accurate modeling of capacitive grids plays an important role in the modeling of the complete surface structure. In general, the modeling of planar metallic screens excited by a plane wave can be categorized into computational and analytical methods. The computational models for conducting screens composed of square or rectangular patches (*e.g.* in [15–18]) are as a rule based on the Floquet expansion of the scattered field. In this doctoral thesis we concentrate on the analytical models that describe the properties of such screens through the averaged electromagnetic fields on the screens.

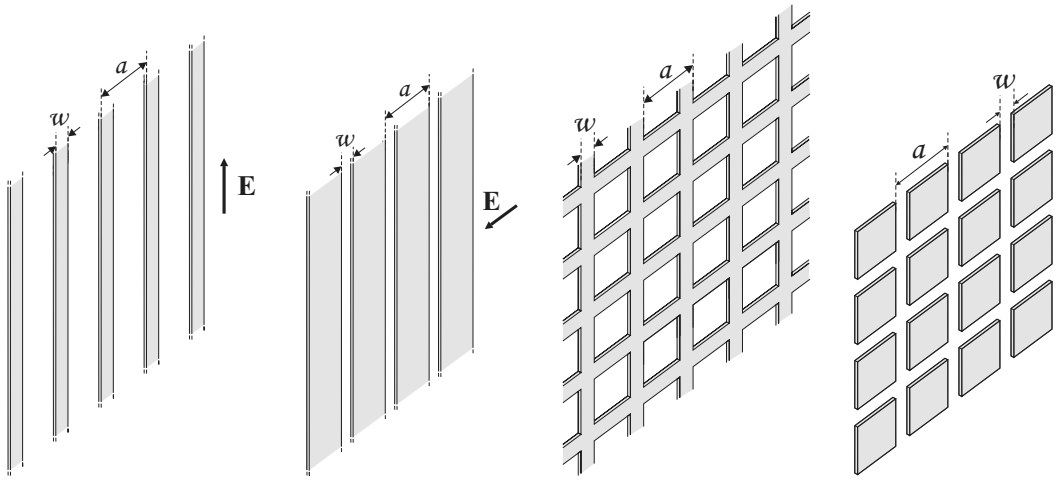

Figure 3.1: (a) Periodically organized grid of parallel strips having an inductive response to the electric fields parallel to the strips and (b) its complementary structure. For the complementary structure the response to the electric field perpendicular to the strips is capacitive. Therefore, the complementary structure is commonly referred to as capacitive grid. Further, (c) inductive mesh and (d) its complementary structure capacitive mesh. Metal parts are colored grey.

The cases of periodically organized thin electrically conductive wires and strips have been studied in the literature since 1890s. An illustration of periodically organized parallel inductive and capacitive strip structures is shown in Fig. 3.1. In the case, when the incident electric field component is parallel to the wires, the response of these structures to the impinging electromagnetic wave is inductive at low frequencies. In general, this condition has been studied more widely in the literature than its complementary structure, where the wire diameter or the strip width is large compared to the periodicity of the structure and the response of the screen is capacitive at low frequencies. Actually, due to this fact, it is convenient to derive the equivalent surface impedance of the capacitive screen through its inductive complementary structure using so-called Babinet's principle (also referred to as Booker's condition [19]). For this reason the properties of some inductive grids and meshes are reviewed in the following. The examination is limited to the structures that serve the purpose of deriving an analytical model for patch arrays or capacitive grids, that is, to inductive grids and bonded meshes.

In the following, the previous work on the analytical modeling of inductive grids and bonded meshes is discussed. The discussion is then extended to the use of Babinet's principle at the interface of two dielectrics and finally to modeling of capacitive strips and meshes. The contributions of this thesis to the modeling of capacitive screens are discussed in the end of this chapter.

3.2 Inductive grids and meshes

Apparently, the first quantitative study on the properties of parallel wire grids was done by Lamb in 1898 [20]. In [20] Lamb used conformal mapping techniques to derive the static field distributions near the grid of parallel wires and used this information as the basis for calculations of the reflection and transmission coefficients for the normal incidence. In [20] it was found that if the wire diameter is small compared to the grid periodicity, the reflection and transmission coefficients are dependent on the periodicity of the grid. Later, in 1914, von Ignatowsky made detailed analysis of the scattering properties of parallel wire grids for oblique incidence and for different materials of the wires [21]. The theory covered also cases when the wavelength is comparable with the periodicity of the grid. After [21], the reflection and transmission properties of parallel wire grids in free space have been studied in [22–29].

MacFarlane [23] showed in 1946, to the best of the author's knowledge, for the first time that the scattering problem of a parallel wire grid can be solved using a transmission-line model, where the wire grid is modeled as a shunt impedance and the homogeneous surrounding medium is modeled as infinite transmission lines. The shunt impedance is proportional to $\ln(a/2\pi r_0) + \Delta$, where a is the periodicity of the grid, r_0 is the radius of the wires, and Δ is a correction factor depending on the incidence angle and periodicity. This relates closely to the approach used in this thesis in modeling of capacitive meshes or artificial impedance surfaces. Wessel [24] and Hornejäger [25] arrived to the same result, but defined the grid impedance differently. Wessel and Hornejärer defined the

grid impedance to be the ratio between the electric field component parallel to the wires and the current of a single wire. The approach of MacFarlane was used later by Wait [26] to take into account the finite conductivity of the wires. Wait found that the finite conductivity of the wires can be taken into account by adding a corresponding impedance in series with the shunt grid impedance of MacFarlane [23]. Correspondingly, in [27] similar finding was done with respect to the grid impedance of [24, 25]. The periodical loading of the wire grid with lumped circuit elements was first proposed by Trentini [28].

As a concluding remark of the discussion so far, the works of MacFarlane [23], Wait [26], and Trentini [28] have developed a general transmission-line model for the case of wire grids in homogeneous media. In its generality, this model covers most of the cases that can be considered for this type of structure. However, the models so far have suffered from an obvious drawback: Namely, they do not take into account the effect of a nearby material interface. In applications such grids are in general constructed on or backed up with dielectric layers. Therefore, knowledge on the effect of the surrounding dielectrics to the properties of the grids becomes important.

In [30] Wait used the transmission-line model for calculating the reflection of a plane wave at oblique incidence on a wire grid parallel to a dielectric interface. More results were later provided in [31] where some of the errors in [30] were corrected. The results in [30, 31] show that a dielectric medium can have a significant effect on the correction factor of the grid impedance and that in the very vicinity of the dielectric interface the value of the correction factor changes rapidly with respect to the distance from the grid to the interface. However, for electrically dense grids ($a/\lambda \ll 1$), the effect remains small. Also, cases when the permeability of the surrounding medium differs from the one in free space [32–34] or when the grid is located at the interface of two magnetic materials [35–37] have been studied.

In the case of inductive metallic meshes, apparently the first derivations of the averaged boundary conditions have been conducted by Kontorovich and Astrakhan in [38, 39]. Independently from Kontorovich and Astrakhan, Ulrich [40] derived the expression for the grid impedance of square wire meshes in free space qualitatively from the formulas presented in [29] for the grid impedance of a parallel wire grid. Ulrich reasoned that for the normal incidence the square mesh can be considered to be composed of two independent grids of wires that for certain polarization have both inductive and capacitive response. Therefore, for the case when $\lambda \gg a \gg r_0$ the response of the inductive mesh should be that of an inductive grid with the same parameters a and r_0. The result of this simple reasoning agrees with the results of [38, 39]. The results of Kontorovich and Astrakhan were later verified by Hill and Wait [41]. In 1982 Lee *et al.* [42] obtained an approximation for the grid impedance for an inductive or capacitive grid mesh in a homogeneous medium at normal incidence by matching a curve to extensive amount of numerical data.

The models for the normal incidence discussed above are of the first order whereas the models for the oblique incidences are of the second order with respect to the tangential spatial derivatives. The accuracy of the models can be increased further by taking into account terms of higher orders. Especially in the cases of large incidence angles or elec-

trically large periodicity of the grid, the use of higher-order approximations increases the accuracy of the model notably. Such conditions have been derived for a parallel wire grid by Yatsenko [43] up to the sixth order.

3.3 Capacitive grids and meshes

One of the earliest equivalent circuit models of capacitive grids can be found in [29]. The expressions for the grid impedance [29] cover TE- and TM-polarized cases for arrays of parallel capacitive strips or wires in homogeneous materials and have been obtained by using an integral equation method. Capacitive meshes, *i.e.* patch arrays, were not considered. The case of capacitive mesh was considered later by Ulrich [44] for the normal incidence[1]. Ulrich reasoned that at low frequencies the inductive grids and meshes as well as the capacitive counterparts should behave similarly. However, experiments had shown that at frequencies when λ becomes approximately equal to the periodicity of the mesh, the capacitive and inductive meshes become resonant. Based on this empirical observation Ulrich improved the equivalent circuits for inductive and capacitive grids for meshes with an additional capacitor and inductor, respectively. The value of these extra circuit elements was evaluated from the measurements by matching the resonance at $\lambda \approx a$ in the circuit model with the measurements. Similarly as for the case of inductive grids and meshes, the accuracy of the models presented in [29, 44] is lost when the gap between the strips is no longer small compared to the strip width.

Following generally the equivalent circuits of Marcuvitz [29] and Ulrich [44], the case of capacitive strips or meshes at a dielectric interface were studied by various authors for the normal incidence in [45–48]. Timusk and Richards [45] took the effect of the dielectric substrate into account by simply considering the elementary parallel combination of two capacitors with different dielectrics. Shanahan and Heckenberg [46], and later Compton *et al.* [47], used instead Babinet's principle to develop an equivalent circuit model for capacitive grids and meshes from their complementary structures. However, the free-space Babinet's principle was not used appropriately in [46], as was pointed out by Compton *et al.* [47]. By correctly using the modified approximate Babinet's principle, the authors of [47] arrived to the same result as Timusk and Richards [45], further verifying the correctness of both results. In [48] some errors in the previously published models were pointed out and corrected models were presented. The importance of the work of Compton *et al.* [47] and Whitbourn [48] arises from the derivation of the approximate Babinet's principle.

Much later, Holloway *et al.* [49] studied the reflection properties of arrays of separate scatterers. As an example, also the case of a square patch array was considered even for the oblique incidence (see also [50]). However, Holloway *et al.* [49] considered the interactions between the separate scatterers to be solely dipole interaction neglecting the capacitive interaction between the adjacent patches. This becomes important when the

[1]Ulrich [44] derived also an equivalent circuit for a capacitive grid from its complementary structure inductive grid by using Babinet's principle.

separation of the adjacent patches becomes small, which is the case in all high-impedance surfaces. Also, in [51] Clavijo *et al.* touched the topic of modeling capacitive meshes while deriving an analytical model for a high-impedance surface. In that work the authors of that paper derived semi-intuitively an expression for the input impedance of a capacitive mesh by treating the mesh as an anisotropic material slab with a finite thickness.

In conclusions of the literature review for the capacitive screens, homogenization models for arrays of capacitive strips are available in the literature, even for oblique incidence. However, models for capacitive square meshes or arrays of patches have been considered only for the normal incidence or for structures where the separation of the adjacent patches is considerably large. Also, semi-intuitive expressions have been derived for the capacitive meshes. The response of the latter structure is nearly isotropic when $\lambda \gg a$ whereas the former structure remains anisotropic even at low frequencies.

3.4 Contributions of this thesis

In the following, the findings of [**I**, **II**] and, especially, how the proposed models physically differ from the previously published models are discussed in more detail.

Let us start from the complementary structure of a capacitive grid, that is from an inductive grid with electrically narrow strips along the x-axis. The plane of incidence lies in the $(x-z)$-plane and the incident wave is polarized so that the transverse electric field component is always along the x-axis. For the normal incidence the phase front of the incident plane wave is parallel to this inductive screen and no phase difference occurs between the current in one place of a strip compared to another. Therefore the current flows uniformly along the strips and the electric charges do not accumulate in any part of the strips. For oblique incidence the phase of the incident electric field component along a strip is different in one place compared to another. Because of this, also the phase of the current varies along the strip and causes charges to accumulate in different parts of the strip. The same phenomenon takes place in all electrically conductive interfaces and naturally has an effect on the averaged transition conditions for oblique incidence. Due to duality, the same physics applies also to the complementary structure of the inductive grid, that is for a capacitive grid. In this case the transverse component of the magnetic field is directed along the gaps between the adjacent strips and the electric surface current is replaced with the magnetic surface current.

In inductive meshes strips directed along the y-axis are bonded with the strips of the inductive grid discussed in the previous paragraph and the plane of incidence remains the same. The strips along the y-axis are at the same potential as the points at which they are bonded to the strips along the x-axis. For the normal incidence the response of the inductive mesh is the same as of the inductive grid. This is because the current flows uniformly and there exists no potential difference on the strips along the x-axis. For oblique incidence different points of the strips directed along the x-axis and the strips

along the y-axis lie at different potentials. Due to the potential differences between the strips in the y-direction and the points of the strips along the x-axis, now current flows also from the orthogonal strips directed along the y-axis to the strips directed along the x-axis, and vice versa. Because of this additional current and Kirchhoff's current law, the current on the strips along the x-axis becomes discontinuous. Again, due to duality of the problems, the same applies also for the capacitive meshes with magnetic fields and surface currents. This has been taken into account in the models derived in [**I**, **II**] for the capacitive grids and meshes, and semi-intuitively also in [51] for capacitive meshes. Other models, such as the ones presented in [44–48] for capacitive meshes, do not take these effects into account in their models for the normal incidence. Also, in [49] a completely different approach is considered that does not involve surface currents at all, but separate scatterers.

3.4.1 Analytical modeling of capacitive grids and meshes at the interface of two dielectric media

Let us consider an inductive mesh formed by parallel strips in two orthogonal directions, as illustrated in Fig. 3.2 (a). The periods of the structure in the x- and y-directions are a and b, respectively. For the case when $a = b$ and the period of the structure a is electrically small, the electromagnetic response of the structure is nearly isotropic and it weakly depends on the plane of incidence. In the case of non-zero electric field components along the direction of the strips and for the case when the strip width is much smaller than the period of the structure ($a, b \gg w$), the response of the mesh is inductive at low frequencies. Averaged boundary conditions for such meshes can be found *e.g.* in [14]. In Fig. 3.2 (b) the complementary structure for the inductive strip mesh is shown. Here, the blank parts of the structure illustrated in Fig. 3.2 (a) are metal. For the structure illustrated in Fig. 3.2 (b) the electromagnetic response of the grid is capacitive at low frequencies, as shall be seen below. Let us consider in the following a case where the incidence plane is in the $(y - z)$-plane. For this case the grid impedance for an array of patches over a dielectric sheet can be derived from the averaged boundary conditions for inductive

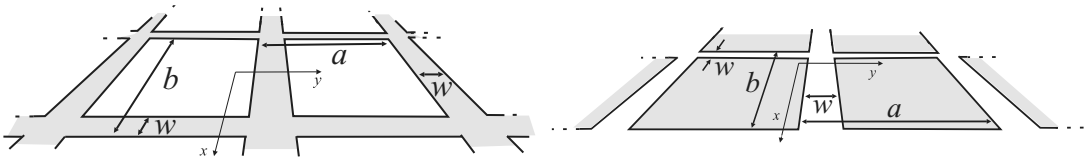

(a) (b)

Figure 3.2: (a) A mesh of ideally conducting strips in homogeneous host medium. (b) Array of patches in homogeneous host medium. Metal parts are colored grey.

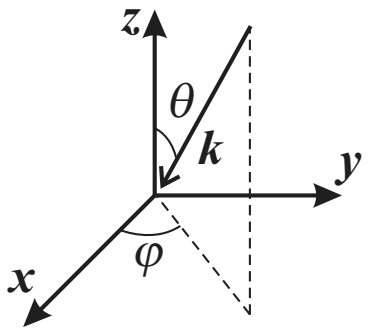

Figure 3.3: The θ and φ angles. In this figure **k** is the wave vector of the incident wave. When the incidence plane is in the $(x-z)$-plane, $\varphi = 0$. Similarly, when the incidence plane is in the $(y-z)$-plane, $\varphi = \pi/2$.

meshes [14] through Babinet's principle and it reads for TM- and TE-fields, respectively, as [**I**,**II**]:

$$Z_{\mathrm{g}}^{\mathrm{TM}} = -j\frac{\eta_{\mathrm{eff}}}{2\alpha_{\mathrm{TM}}}, \tag{3.1}$$

$$Z_{\mathrm{g}}^{\mathrm{TE}} = -j\frac{\eta_{\mathrm{eff}}}{2\alpha_{\mathrm{TE}}\left(1-\frac{k_0^2}{k_{\mathrm{eff}}^2}\frac{\sin^2\theta}{1+\frac{b}{a}}\frac{b}{a}\right)}, \tag{3.2}$$

where the effective wave impedance $\eta_{\mathrm{eff}} = \frac{\eta_0}{\sqrt{\varepsilon_{\mathrm{eff}}}}$, the effective wave number $k_{\mathrm{eff}} = k_0\sqrt{\varepsilon_{\mathrm{eff}}}$, θ is the angle of incidence (see Fig. 3.3), and b and a are the dimensions of the unit cell of the structure along the $x-$ and $y-$axes, respectively. Further, α is the *grid parameter* and it reads for the TM- and TE-polarized cases, respectively, as:

$$\alpha_{\mathrm{TM}} = \frac{k_{\mathrm{eff}}a}{\pi}\ln\left(\frac{1}{\sin\left(\frac{\pi w}{2a}\right)}\right), \tag{3.3}$$

$$\alpha_{\mathrm{TE}} = \frac{k_{\mathrm{eff}}b}{\pi}\ln\left(\frac{1}{\sin\left(\frac{\pi w}{2b}\right)}\right), \tag{3.4}$$

where w is the gap between the adjacent patches (see Fig. 3.1 (b)). In the case $a = b$ the mesh is isotropic and above expressions for the grid parameters are the same for the TM and TE fields. The effective relative permittivity for an array of patches or a grid of strips on a boundary between two media having the relative permittivities of ε_1 and ε_2 reads approximately [47]:

$$\varepsilon_{\mathrm{eff}} = \frac{\varepsilon_1+\varepsilon_2}{2}. \tag{3.5}$$

The grid impedance for a capacitive grid shown in Fig. 3.3 (b) reads for TM- and TE-fields, respectively, as [**I**]:

$$Z_{\mathrm{g}}^{\mathrm{TM}} = -j\frac{\eta_{\mathrm{eff}}}{2\alpha_{\mathrm{TM}}}, \tag{3.6}$$

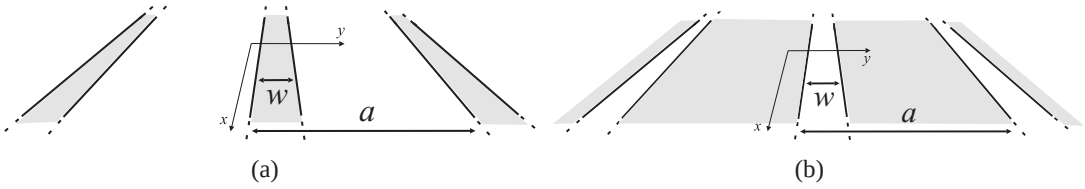

Figure 3.4: (a) An inductive grid of ideally conducting strips in homogeneous host medium. (b) A capacitive grid of ideally conducting strips in homogeneous host medium. Metal parts are colored grey.

$$Z_{\mathrm{g}}^{\mathrm{TE}} = -j\frac{\eta_{\mathrm{eff}}}{2\alpha_{\mathrm{TE}}}\frac{1}{\left(1-\frac{k_0^2}{k_{\mathrm{eff}}^2}\sin^2\theta\right)}. \tag{3.7}$$

Eqs. (3.6) and (3.7) correspond to the results presented in [29] for an array of capacitive strips. Care should be taken when using expressions (3.6) and (3.7) since for different polarizations the plane of incidence varies. Following the notations in Fig. 3.4, for the TE-polarized case the plane of incidence is the $(x-z)$ plane whereas for the TM-polarized fields the incidence plane is the $(y-z)$ plane.

Expressions (3.1)-(3.2) and (3.6)-(3.7) are valid for the cases when $a, b/\lambda \leq 0.5$. The validity range of the expression for the grid impedance can be extended by using a higher-order approximation for the grid parameter. In [43] the accuracy of the higher-order approximation for sparse wire grids was shown to be good up to the frequencies where $a, b \approx \lambda$. The ultimate limit for the validity of (3.1) and (3.2) is $a, b = \lambda$ for the normal incidence. After this limit the fields at the screen become too quickly oscillating and averaging fails. After the limit $a, b = \lambda$ grating lobes emerge and the characterization of the surface with a single surface impedance is not adequate.

3.4.2 Numerical verification and comparison to existing results

In [**I**] the analytical results for the capacitive mesh were verified numerically. As an example, an array of square patches in free space was considered. The dimensions of the array were chosen to be $a = b = \lambda/10$ and $w = a/10$. The reflection coefficient of such structure as the function of the incidence angle is given in Fig. 3.5. The reflection coefficient of the array can be calculated from a transmission-line model, where the shunt grid impedance Z_{g} is in between two infinite transmission lines whose characteristic impedances equal to the free-space impedance for the same plane as the patch array. The results according to (3.1) and (3.2) are compared with the results of Holloway *et al.* [49]. Comparison is made also with numerical results based on the Fourier modal method developed by Granet and Plumey [52] and used in [53] for analysis of strip grat-

ings. The agreement between the grid impedance model presented in (3.1) and (3.2) and the numerical results is very good. The results compare well also against the alternative analytical model [49], although the agreement with the numerical results is slightly better with the present model.

3.5 Summary of related publications

In [**I**] the analytical models for the capacitive grids and meshes at the interface of two media are derived (see also [**II**] for a more general solution). This has been done strictly following Maxwell's equations, starting from the corresponding complementary structures through Babinet's approximate principle, that is from solutions for inductive grids and meshes. The averaged boundary conditions for these inductive structures have been studied widely in the literature, as discussed earlier. The resulted averaged boundary conditions for the capacitive grids and meshes are accurate even for oblique incidence and for small separation between the adjacent patches or strips. In the case of the capacitive grids the results are equivalent to those in [29] obtained by integral equation method.

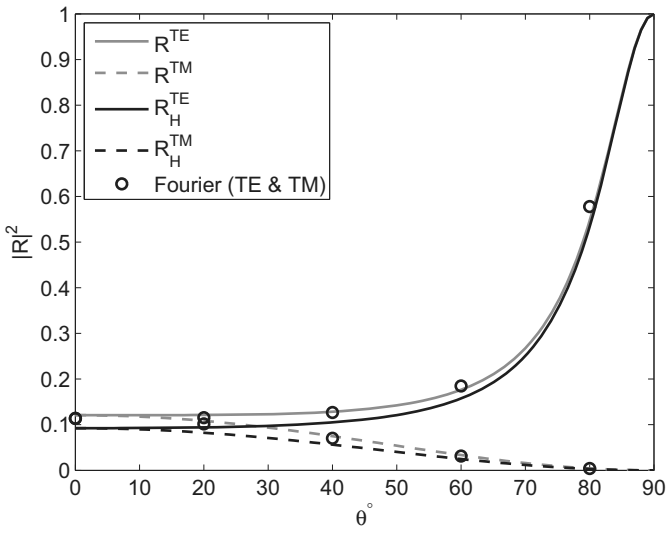

Figure 3.5: The TE- and TM-reflection coefficient versus the incident angle for an array of square patches. The dimensions of the array are the following: $a = b = \lambda/10$ and $w = a/10$. R_{H} corresponds to the results according to the model by C. L. Holloway [49].

4 Analytical modeling of artificial impedance surfaces

4.1 Introduction

The notion “artificial impedance surface” includes all the artificial structures that are designed to operate as a surface with a given impedance response. For instance, corrugated surfaces [54–57] that are composed of series of vertical slots cut into metal, can be considered as an artificial impedance surface when the number of slots per wavelength is large. In this doctoral thesis the analysis concentrates on so-called mushroom structures with or without vertical wires and on structures composed of an array of metallic wires. Such an array of periodically repeated metallic wires, where the periodicity of the structure is much smaller than the wavelength, can be treated also as a medium with certain constitutive material parameters ε and μ. For this reason such a structure is referred also as a wire medium. An illustration of a mushroom structure without vertical wires, a grounded slab of wire medium, and a mushroom structure with vertical wires is given in Figs. 4.1 (a), (b), and (c), respectively.

In the simplest type of a high-impedance surface a capacitive mesh lies over a grounded dielectric slab, as shown in Fig. 4.1. The principle of operation is that the capacitive response of the screen together with the inductive response of the grounded material slab form a resonant structure. The modeling of this type of a structure is rather straightforward and the analysis of Chapter 3 of the capacitive strips and meshes becomes useful (this, of course, applies generally to all structures composed of these capacitive screens). In the more complicated structure, where the dielectric slab is perforated with metallic wires, one can consider the mushroom surface to be composed of a capacitive grid over a grounded wire medium slab. The analogy becomes apparent in Fig. 4.1. Therefore it is convenient to treat the subject of the wire medium and especially the impedance boundary conditions for such structure before discussing the models for the artificial impedance surfaces considered in this thesis.

In what follows, analytical models for different types of high-impedance surfaces are discussed. Before this, however, the properties of the wire medium and grounded wire medium slabs are reviewed. The contributions of this thesis to the modeling of the considered artificial impedance surfaces, or mushroom structures, are discussed at the end of this chapter.

4.2 Artificial dielectrics: Wire medium

Wire medium is a structure that consists of a periodically organized lattice of parallel wires with the lattice constant (or periodicity) a and the wire radius r_0, as shown in Fig. 4.2. Naturally, in order to justify the treatment of the structure as a homoge-

nized medium, the lattice constant needs to be much smaller than the wavelength. In Fig. 4.2 an illustration of a one-dimensional wire medium is shown, but also two- or

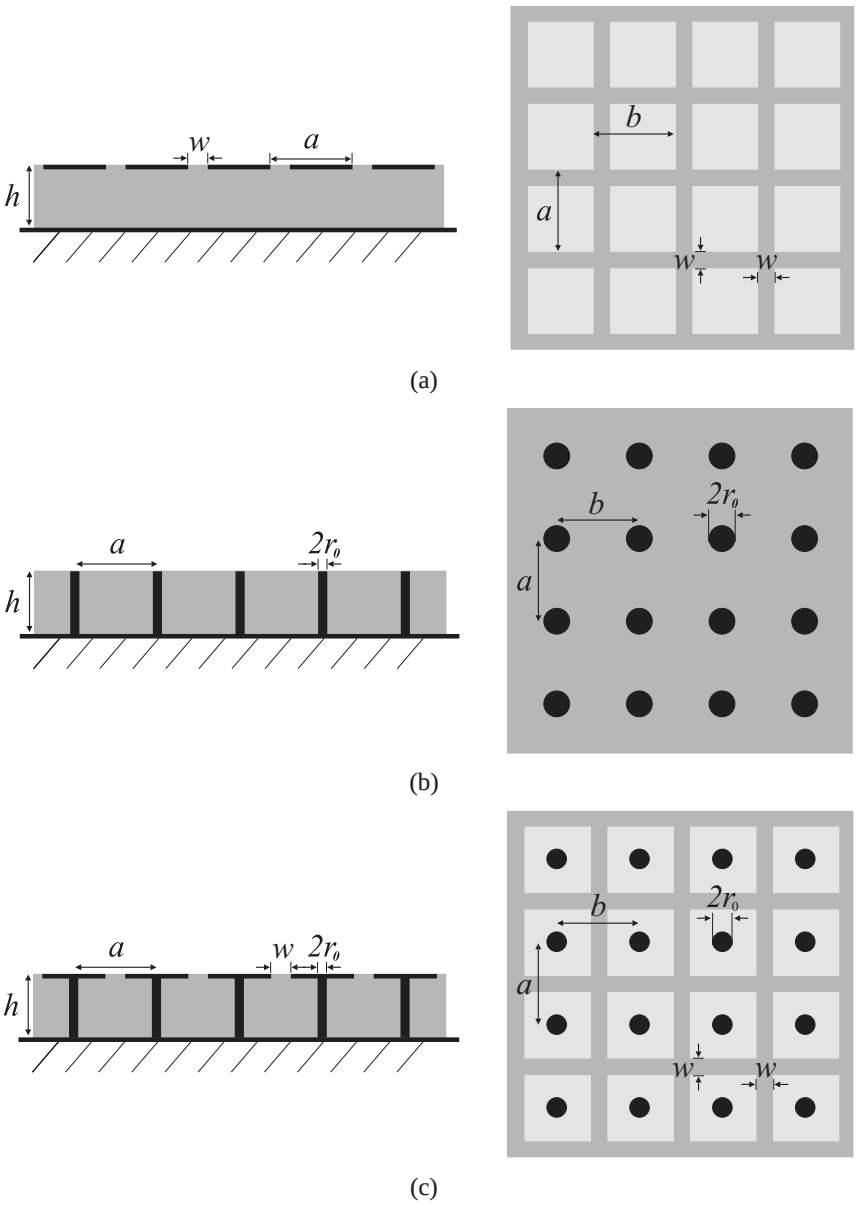

Figure 4.1: (a) A side and top view of mushroom-type artificial impedance surface without metallic wires in the substrate. (b) A side and top view of a grounded wire medium slab. (c) A side and top view of mushroom-type structure with metallic wires in the substrate (also known as the Sievenpiper mushroom structure [79]). This structure can be considered to be composed of the structures shown in (a)-(b).

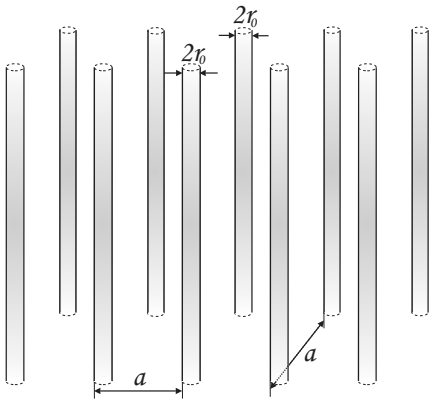

Figure 4.2: An infinite lattice of periodically organized wires.

three-dimensional structures are possible. The wire medium (or rodded medium) was first studied by Brown [58] in 1953 in the context of microwave lenses. The purpose was to make use of the low-loss and dielectric constant below unity properties of the artificial dielectric material (see also [59–62]). In his work Brown derived expressions for the refractive index of a wire medium composed of perfectly conducting wires aligned parallel with the exiting electric field. Later Rotman [63] used the wire medium for simulating plasma and expanded the analysis of Brown to cover wires made of resistive materials.[2] Both Brown [58] and Rotman [63] made use of the transmission-line formalism in their studies, but also electromagnetic mixing formulas can be used to characterize wire medium [62] (more about electromagnetic mixing formulas in general can be found in [64]).

In 1983 King *et al.* [65] derived an expression for the grounded wire medium slab or "Fakir's bed of nails" shown in Fig. 4.1 (b). The same structure had been experimentally investigated earlier by Kay [66] and Querido [67]. King [65] showed that in the case when the lattice constant is sufficiently small with respect to the operational wavelength and the medium is below cut-off, the surface impedance of the grounded wire medium slab becomes independent of the incidence angle. In this case one can consider the parallel wires to behave as shorted TEM transmission lines whose length is equal to the thickness of the dielectric layer [14].

Recently, the spatially dispersive properties of the wire medium have been studied in [68–70]. Accurate analysis reveals that the structure is spatially dispersive (the medium is characterized using non-local material parameters). In the context of grounded wire medium slabs, the spatially dispersive properties of the wire medium have been taken into account in recent works of Silveirinha [71–73]. While trying to solve the elec-

[2]Being similar problems with the modeling of grids discussed in the previous chapter, it is interesting to see the analogy between the works of Brown [58] and Rotman [63], and MacFarlane [23] and Wait [26].

tromagnetic fields in the wire medium slabs, the spatially dispersive properties of wire media include an extra variable into the expressions. Therefore, the classical boundary conditions are not sufficient in order to solve the problem unambiguously and additional boundary conditions are needed. In [71] an additional boundary condition at the interface of air and wire medium was derived. Later, Silveirinha [72] derived an additional boundary condition also for the interface of metal and wire medium. These additional boundary conditions were used in [73] to derive a closed-form expression for the surface impedance of a grounded wire medium slab (the structure shown in Fig. 4.1 (b)).

Also the suppression of spatial dispersion in wire medium has been studied recently. Interestingly, it has been found that in mushroom structures the spatial dispersion can be suppressed when the structure is electrically thin [2, 3]. This result is in good agreement with the findings of [74], where it was also noticed that the spatially dispersive properties of wire medium become nearly negligible when effective capacitance between the wires is increased. In such cases the wire medium can be modeled as a uniaxial material with local material parameters (spatially non-dispersive).

4.3 Analytical models for the artificial impedance surfaces in the literature

The artificial impedance surface structures composed of patch arrays excluding vertical vias have been first proposed in [75–77], whereas the similar artificial impedance surface including vertical wires, *i.e.*, a mushroom structure, has been proposed in [78, 79]. No quantitative models for the high-impedance surface structures were presented in [76, 77]. In their analysis of the surface Liu *et al.* used numerical methods based on the Floquet expansions of the fields on the surface of the structure. In [77] a schematic illustration of the equivalent-circuit model was given for qualitative understanding of the properties of the newly proposed structure. A similar circuit model to that of [77] for a mushroom structure with vertical metallic wires was proposed by D. Sievenpiper in [78]. Here the capacitance of the patch array formed a parallel resonant circuit with the inductance of the grounded dielectric slab. The capacitance in this model was calculated through the quasi-static approximation for a gap between two semi-infinite strips. No phase variation in any of the transverse directions was taken into account. The approximation for the inductance in [78] assumes constant magnetic field magnitude over the height of the structure and holds only for electrically thin structures. Furthermore, the effect of the vertical metallic wires is not taken into account. In [51] the Sievenpiper high-impedance surface was modeled in terms of layered homogeneous materials with anisotropic magneto-dielectric tensors. The resulting expressions for the surface impedance of high-impedance surfaces are lengthy and complicated. Although the validity of the approach of treating an array of rectangular patches as a thin slab of anisotropic material remains debatable, the authors of [51] touch the topic of grid impedance of an array of patches without treating it in more detail. The grounded dielectric slab with metallic vias was treated in [51] as a slab of wire medium, as was also done in [14, 80]. In [14, 80, 81] the models for the square patch array

neglected the periodicity of the array in the other direction or were derived for the normal incidence.

So far we have discussed artificial impedance surface structures composed of square patch arrays which at low frequencies are nearly isotropic. However, also anisotropic structures, composed of capacitive strips, have been proposed. Higgins *et al.* [82] considered a high-impedance surface comprising an array of parallel capacitive strips over a grounded dielectric slab perforated with metallic vias. The main emphasis in [82] was to make the frequency response of the surface electrically tunable and only a schematic illustration of the equivalent circuit model was presented. In fact, for the normal incidence the electromagnetic response from an array of strips for one polarization (electric field orthogonal to the strips) is exactly the same as from an array of patches.[3] Therefore one can argue that for the structure proposed in [82] for the normal incidence and for the polarization where the electric field is orthogonal to the strips the models were published already in [14, 51, 80, 81]. Furthermore, although the models in [14, 80] were derived for high-impedance surfaces with patches, they are actually applicable for high-impedance surfaces with strips due the fact that the periodicity in one of the directions is neglected, as shall be seen later in the following subsections.

Also the possibility to mechanically or electrically tune the artificial impedance surfaces has been studied. In [83] Sievenpiper *et al.* demonstrated a simple way of mechanically tuning the direction of the main beam of a reflector-type antenna. In that paper the capacitive grid of an artificial impedance surface was formed with two overlapping patch arrays. The effective capacitance was then tuned by mechanically sliding the upper array and changing the overlapping area. Although in practical applications this approach might not be feasible, the method of varying the effective grid capacitance of the artificial impedance surface for tuning has been used in many following papers. In [84] Sievenpiper *et al.* used the same method for electrically tunable artificial impedance surfaces in reflector-type antennas. In [84] the capacitance formed between the adjacent patches of the capacitive mesh was tuned by voltage controllable varactors. By forming a certain gradient for the effective capacitance the reflection phase of the surface could be changed and the direction of the main beam tuned. Later this was done for leaky-wave antennas with mechanically [85] and electrically [86] tunable effective capacitances. In [84] some of the vertical metallic vias were used to bring bias voltage for the varactors. Also different type of bias networks have been proposed [87]. In [87] Mias *et al.* also proposed a lumped element model for the mushroom structure for the normal incidence.

In conclusions of the literature review on the analytical modeling of artificial impedance surfaces, for artificial impedance surfaces with capacitive strips or arrays of patches, no physically strict analytical models have been presented in the open literature for oblique incidence.

[3] Considering the principle of operation of high-impedance surfaces, this is the more interesting polarization since the response of grid of strips for this polarization is capacitive.

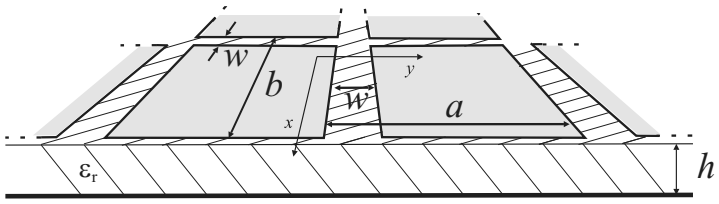

Figure 4.3: An artificial impedance surface composed of an array of patches over a grounded dielectric slab.

4.4 Contributions of this thesis

In the following the results of the thesis relating to this topic are shortly presented. First, analytical models for the artificial impedance surfaces are presented. We start from the analytical models for the structures composed of a capacitive screen over a grounded dielectric slab. We will then consider structures in which the grounded dielectric slab is perforated with vertical metallic wires. Also, electrically tunable surface structures are considered. After this, we will discuss what kind of effective material parameters are needed for an uniaxial material slab in order to realize artificial magnetic conductors. Finally, the analytical models are verified with simulations and in some cases with experiments.

4.4.1 Analytical model for the artificial impedance surface composed of a capacitive grid over a grounded dielectric slab

Let us consider an artificial impedance surface that is composed of a capacitive grid or mesh (considered in section 3.4.1) over a grounded dielectric slab. In Fig. 4.3 a case of an array of patches over a grounded dielectric slab is shown (this corresponds also to the case in Fig. 4.1(a)). For this type of structure it is convenient to model the system by using the transmission-line formalism. An equivalent transmission-line model for the artificial impedance surface structure is shown in Fig. 4.4. In the transmission-line model, the surface impedance of the artificial impedance surface at the interface of the capacitive grid Z_{inp} can be calculated as a parallel connection of the grid impedance Z_{g} and the surface impedance of the grounded dielectric slab Z_{d} at the grid interface:

$$Z_{\mathrm{s}}^{-1} = Z_{\mathrm{g}}^{-1} + Z_{\mathrm{d}}^{-1}. \tag{4.1}$$

Further, Z_0 is the free-space impedance that reads for the TM and TE fields, respectively, as

$$Z_0^{\mathrm{TM}} = \eta_0 \cos(\theta), \tag{4.2}$$

$$Z_0^{\mathrm{TE}} = \frac{\eta_0}{\cos(\theta)}, \tag{4.3}$$

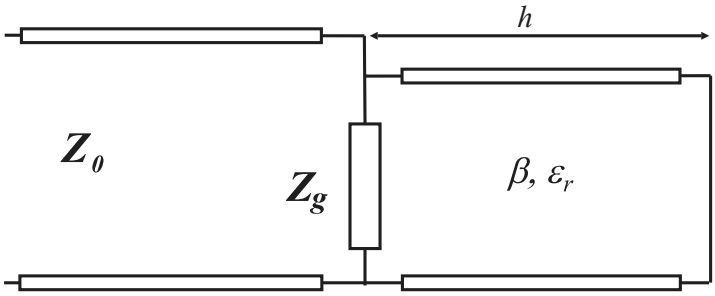

Figure 4.4: An equivalent transmission-line model for the artificial impedance surface.

where η_0 is the plane-wave impedance in free space and θ is the incidence angle. The grid impedances are given for the TM- and TE-polarized cases in (3.1) and (3.2) in the case of capacitive arrays of metal patches, and in (3.6) and (3.7) in the case of capacitive grids, respectively. The surface impedance of the grounded dielectric slab can be written in dyadic form as

$$\overline{\overline{Z}}_{\mathrm{s}} = j\omega\mu \frac{\tan(\beta h)}{\beta} \left(\overline{\overline{I}}_{\mathrm{t}} - \frac{\mathbf{k}_{\mathrm{t}}\mathbf{k}_{\mathrm{t}}}{k^2} \right), \tag{4.4}$$

where μ is the absolute permeability of the substrate (in our case $\mu = \mu_0$), $\beta = \sqrt{k^2 - k_{\mathrm{t}}^2}$, $k = k_0\sqrt{\varepsilon_{\mathrm{r}}}$ is the wave number in the substrate material, ε_{r} is the permittivity of the material, h is the height of the material slab, and $\mathbf{k}_{\mathrm{t}}$ is the tangential wave number component, as imposed by the incident wave.

From (3.1), (3.2), and (4.1) we get for the surface impedance of the artificial impedance surface composed of a capacitive mesh over a grounded dielectric slab [I]

$$Z_{\mathrm{s}}^{\mathrm{TM}} = \frac{j\omega\mu \frac{\tan(\beta h)}{\beta} \cos^2(\theta_2)}{1 - 2k_{\mathrm{eff}}\alpha_{\mathrm{TM}} \frac{\tan(\beta h)}{\beta} \cos^2(\theta_2)}, \tag{4.5}$$

$$Z_{\mathrm{s}}^{\mathrm{TE}} = \frac{j\omega\mu \frac{\tan(\beta h)}{\beta}}{1 - 2k_{\mathrm{eff}}\alpha_{\mathrm{TE}} \frac{\tan(\beta h)}{\beta} \left(1 - \frac{k_0^2}{k_{\mathrm{eff}}^2} \frac{\sin^2\theta}{1 + \frac{b}{a}} \frac{b}{a} \right)}, \tag{4.6}$$

where θ_2 is the angle of refraction calculated from the law of refraction as $\theta_2 = \arcsin\left(\sin(\theta)/\sqrt{\varepsilon_{\mathrm{r}}}\right)$, $k_{\mathrm{eff}} = k_0\sqrt{\varepsilon_{\mathrm{eff}}}$ is the effective wave number, $\varepsilon_{\mathrm{eff}} = (\varepsilon_{\mathrm{r}} + 1)/2$ is the effective relative permittivity, and $\alpha_{\mathrm{TM,TE}}$ is the grid parameter given by (3.3) and (3.4) for the TM and TE fields, respectively. Further, a and b are the periodicity of the capacitive mesh as given in Fig. 4.4.

Similarly, from (3.6), (3.7), and (4.1) we get for the surface impedance of the artificial impedance surface composed of a capacitive grid of metal strips over a grounded dielectric

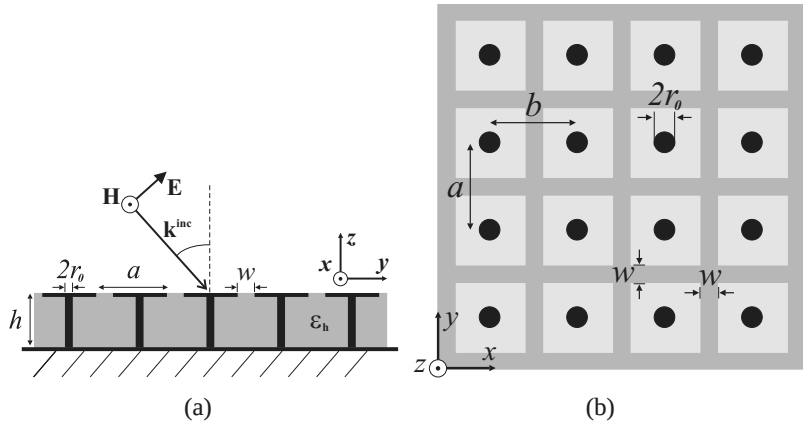

(a) (b)

Figure 4.5: Illustration of the mushroom structure (a) from the side and (b) from above. The structure comprises a patch array over a dielectric slab perforated with metallic vias. The gap between the adjacent patches is w and $\varepsilon_{\rm r}$ is the relative permittivity of the host medium.

slab [I]

$$Z_{\rm s}^{\rm TM} = \frac{j\omega\mu\frac{\tan(\beta h)}{\beta}\cos^2(\theta_2)}{1-2k_{\rm eff}\alpha_{\rm TM}\frac{\tan(\beta h)}{\beta}\cos^2(\theta_2)}, \tag{4.7}$$

$$Z_{\rm s}^{\rm TE} = \frac{j\omega\mu\frac{\tan(\beta h)}{\beta}}{1-2k_{\rm eff}\alpha_{\rm TE}\frac{\tan(\beta h)}{\beta}\left(1-\frac{2}{\varepsilon_{\rm r}+1}\sin^2\theta\right)}. \tag{4.8}$$

4.4.2 Analytical model for the artificial impedance surface composed of a capacitive grid over a grounded dielectric slab perforated with metallic vias

Let us now consider a mushroom structure shown in Fig. 4.5. For TE fields the electric field is always perpendicular to the wires. If the radius of the wires is very small, the electric field does not excite them and the wire medium slab appears for the TE fields as a grounded dielectric slab. Therefore, it can be concluded that for the TE fields the analytical models derived for the artificial impedance surfaces in section 4.4.1 are also applicable for the mushroom structures. However, for TM-polarized oblique incidence the electric field component parallel to the vertical wires excites them. For this polarization the effect of the wires needs to be taken into account. In the following analysis for the TM fields it is considered that the mushroom structure is comprised of a capacitive patch array and an effective grounded wire medium slab.

Following the lay-out of [II], in the case when the mushroom structure is electrically thin, the wire medium can be considered to be uniaxial with local material parameters. In this

case the surface impedance for the grounded uniaxial material slab reads [14]:

$$Z_{\mathrm{d}}^{\mathrm{TM}} = j\omega\mu_0 \frac{\tan(\beta_{\mathrm{TM}} h)}{\beta_{\mathrm{TM}}} \frac{k^2 - k_{\mathrm{t}}^2 - k_{\mathrm{p}}^2}{k^2 - k_{\mathrm{p}}^2}, \tag{4.9}$$

where

$$\beta_{\mathrm{TM}}^2 = \omega^2 \varepsilon_0 \varepsilon_{\mathrm{r}} \mu_0 - \frac{\varepsilon_{\mathrm{r}}}{\varepsilon_{\mathrm{n}}} k_{\mathrm{t}}^2, \tag{4.10}$$

and k_{p} is the plasma wave number given for an arbitrary lattice ($r_0 \ll a, b$) as [70]

$$\left(k_{\mathrm{p}}\sqrt{ab}\right)^2 = \frac{2\pi}{\ln\left(\frac{\sqrt{ab}}{2\pi r_0}\right) + F(a/b)}, \tag{4.11}$$

where

$$F(a/b) = -\frac{1}{2}\ln(a/b) + \sum_{\mathrm{n}=1}^{+\infty} \left(\frac{\coth\left(\pi n \frac{a}{b}\right) - 1}{n} \right) + \frac{\pi a}{6b}. \tag{4.12}$$

For a square lattice $F|_{a=b} = 0.5275$. Furthermore, a and b are the periods of the wires and the patches in the y- and x-directions, respectively, r_0 is the radius of the wires, and the local approximation for the relative permittivity for the fields along the normal of the medium reads

$$\varepsilon_{\mathrm{n}} = \varepsilon_{\mathrm{r}} \left(1 - \frac{k_{\mathrm{p}}^2}{k_0^2 \varepsilon_{\mathrm{r}}} \right). \tag{4.13}$$

Now, using (3.1) and (4.9) we get for the surface impedance of electrically thin mushroom structures [II]

$$Z_{\mathrm{s}}^{\mathrm{TM}} = \frac{j\omega\mu_0 \frac{\tan(\beta_{\mathrm{TM}} h)}{\beta_{\mathrm{TM}}} \left(1 - \frac{\sin^2(\theta)}{\varepsilon_{\mathrm{n}}}\right)}{1 - 2k_{\mathrm{eff}} \alpha_{\mathrm{TM}} \frac{\tan(\beta_{\mathrm{TM}} h)}{\beta_{\mathrm{TM}}} \left(1 - \frac{\sin^2(\theta)}{\varepsilon_{\mathrm{n}}}\right)}. \tag{4.14}$$

If the electrical thickness of the mushroom structure is no longer small, the effects of the spatial dispersion in the wire medium need to be taken into account. In this case the wire medium slab can no longer be considered to be uniaxial with local effective material parameters, but the contribution from both TM and TEM modes excited in the wire medium by the incident TM fields has to be considered. However, using the additional boundary conditions, the fields at the interface of the mushroom structure and air can be solved. The reflection coefficient ρ of the mushroom structure for the magnetic fields follows from this theory and it reads [III]

$$\rho = \frac{\frac{\varepsilon_{\mathrm{n}}^{\mathrm{TM}}}{\gamma_{\mathrm{TM}}} \coth(\gamma_{\mathrm{TM}} h) + \frac{\varepsilon_{\mathrm{n}}^{\mathrm{TM}} - \varepsilon_{\mathrm{r}}}{k} \cot(kh) + \frac{\eta_0}{jk_0} Z_{\mathrm{g}}^{-1} - \frac{1}{jk_{\mathrm{z}}}}{\frac{\varepsilon_{\mathrm{n}}^{\mathrm{TM}}}{\gamma_{\mathrm{TM}}} \coth(\gamma_{\mathrm{TM}} h) + \frac{\varepsilon_{\mathrm{n}}^{\mathrm{TM}} - \varepsilon_{\mathrm{r}}}{k} \cot(kh) + \frac{\eta_0}{jk_0} Z_{\mathrm{g}}^{-1} + \frac{1}{jk_{\mathrm{z}}}}, \tag{4.15}$$

where $k_{\mathrm{z}} = \sqrt{k_0^2 - k_{\mathrm{t}}^2}$, $\gamma_{\mathrm{TM}} = \sqrt{k_{\mathrm{p}}^2 + k_{\mathrm{t}}^2 - k^2}$, and the relative effective permittivity along the direction of the metallic vias is written for the TM polarization as

$$\varepsilon_{\mathrm{n}}^{\mathrm{TM}} = \varepsilon_{\mathrm{r}} \left(1 - \frac{k_{\mathrm{p}}^2}{k_{\mathrm{p}}^2 + k_{\mathrm{t}}^2} \right). \tag{4.16}$$

Both expressions (4.14) and (4.15) are valid only for plane waves. For both (4.14) and (4.15) the validity range is defined by the validity ranges of expressions (3.1)-(3.2) and (3.5)-(3.6), respectively. Furthermore, the radius of the wires $r_0 \ll a$. In addition, for (4.14) the height of the mushroom structure needs to be electrically thin: $\lambda \gg h$.

4.4.3 Varactor-tunable artificial impedance surface

As discussed earlier, commonly the electrically tunable artificial impedance surfaces are realized by using varactors to vary the effective capacitance between the adjacent patches or strips. It is possible to take this additional capacitance due to the varactors into account in the analytical models for the different types of artificial impedance surfaces. In capacitive grids and meshes the averaged effective capacitance is formed due to small gaps in the screen. By connecting varactors over these gaps, we actually connect an additional capacitance in parallel with the averaged effective capacitance. Therefore, the grid impedances in (3.1)-(3.2) and (3.5)-(3.6) for capacitive meshes and grids, respectively, can be rewritten to take the additional capacitance into account as [II]

$$Z_{\mathrm{g}}^{\mathrm{TM,TE}} = \frac{1}{j\omega \left(C_{\mathrm{g}}^{\mathrm{TM,TE}} + C_{\mathrm{var}} \right)}, \tag{4.17}$$

where indices TM and TE refer to the polarization, C_{var} is the capacitance of the varactor, and C_{g} is the effective averaged capacitance of the grid written in a lumped element form. Following the notations in Fig. 3.2, the grid capacitance for ideally conducting capacitive mesh reads for TM and TE fields, respectively, as [II]

$$C_{\mathrm{g}}^{\mathrm{TM}} = \frac{a\varepsilon_0 \left(\varepsilon_1 + \varepsilon_2 \right)}{\pi} \ln \left(\frac{1}{\sin\left(\frac{\pi w}{2a} \right)} \right), \tag{4.18}$$

$$C_{\mathrm{g}}^{\mathrm{TE}} = \frac{b\varepsilon_0 \left(\varepsilon_1 + \varepsilon_2 \right)}{\pi} \ln \left(\frac{1}{\sin\left(\frac{\pi w}{2b} \right)} \right) \left(1 - \frac{k_0^2}{k_{\mathrm{eff}}^2} \frac{\sin^2 \theta}{1 + \frac{b}{a}} \frac{b}{a} \right). \tag{4.19}$$

4.4.4 Grounded uniaxial material slabs

In the context of uniaxial material slabs, let us consider a general case of grounded uniaxial material slabs. The uniaxial symmetry of a structure is the most general allowed symmetry, if the surface plane should be isotropic. Here the uniaxial symmetry is considered with a view to simplify the realization of an all-angle magnetic wall when compared to the realization of a magnetic wall with fully isotropic materials. A schematic picture of the grounded uniaxial material slab is shown in Fig. 4.6. In the following, analytical models derived in [IV] for the analysis of the proposed structure are reviewed. Further, the needed material parameters for the realization of an all-angle magnetic wall for the TM fields and practical structures for this polarization are discussed. For the TE fields the

use of uniaxial symmetry does not offer as promising benefits as for the TM fields and the discussion regarding the TE fields can be found in [IV].

It is convenient to model the properties of the structure illustrated in Fig. 4.6 with a surface impedance at the interface of the uniaxial material and air. This can be done using a transmission-line model similar to that in Fig. 4.4. Instead of just one isotropic effective material parameter ε_{r} in Fig. 4.4, we have the effective transverse and normal permittivities (ε_{t} and ε_{n}) and permeabilities (μ_{t} and μ_{n}), respectively. Using the transmission-line model, the local approximation of the surface impedance for the TM and TE fields can be written, respectively, as [IV]

$$Z_{\mathrm{s}}^{\mathrm{TM}} = j\frac{\beta_{\mathrm{TM}}}{\omega\varepsilon_{\mathrm{t}}}\tan\left(\beta_{\mathrm{TM}}h\right), \tag{4.20}$$

$$Z_{\mathrm{s}}^{\mathrm{TE}} = j\frac{\omega\mu_{\mathrm{t}}}{\beta_{\mathrm{TE}}}\tan\left(\beta_{\mathrm{TE}}h\right), \tag{4.21}$$

where h is the height of the slab and the normal components of the wave numbers in the uniaxial material slab read for the TM and TE fields, respectively, as

$$\beta_{\mathrm{TM}}^2 = \omega^2\varepsilon_{\mathrm{t}}\mu_{\mathrm{t}} - k_{\mathrm{t}}^2\frac{\varepsilon_{\mathrm{t}}}{\varepsilon_{\mathrm{n}}}, \tag{4.22}$$

$$\beta_{\mathrm{TE}}^2 = \omega^2\varepsilon_{\mathrm{t}}\mu_{\mathrm{t}} - k_{\mathrm{t}}^2\frac{\mu_{\mathrm{t}}}{\mu_{\mathrm{n}}}. \tag{4.23}$$

Here, k_{t} is the transverse wave number.

In [IV] it was shown that especially for TM fields the realization of the magnetic wall effect becomes simple. For this polarization it is possible to realize a magnetic wall just by letting $\varepsilon_{\mathrm{n}} \to 0$. For $\varepsilon_{\mathrm{n}} > 0$ the surface would not support TM-polarized surface waves nor would the magnetic wall effect be periodic with respect to the frequency. However, for

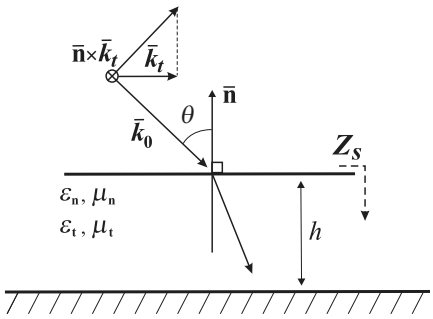

Figure 4.6: An illustrative picture of the grounded uniaxial material slab. Index t corresponds to the direction tangential to the interfaces, and index n marks the components along the unit vector $\mathbf{n}$.

$\varepsilon_{\rm n} < 0$ the electromagnetic response of the surface would becomes a quickly oscillating function of ω.

One possible example of a crystal with near zero values for the effective permittivity is the wire medium. Close to the plasma frequency of the wire medium, the effective permittivity of the material approaches zero. Also, the structure of the wire medium is readily anisotropic so that the uniaxial symmetry is easily attainable. However, in practice the frequency band of the operation will be limited due to the finite band of the plasma resonance. For the proposed structure for the TM fields the wires should be oriented in the vertical direction, similarly to the "Fakir's bed of nail's" structures.

The wire medium is known to exhibit spatial dispersion. However, the above analysis is based on the local approximation of the uniaxial material. Therefore the spatial dispersion in the wire medium needs to be suppressed in order to realize the proposed features of the grounded uniaxial material slab as an artificial magnetic wall. This is possible either by coating the wires with high-μ material [74] or by increasing the capacitance between the wires [2, 3, 74].

It is interesting to notice that that this study pertains closely to the recent studies on the new electromagnetic boundary conditions for anisotropic materials by Lindell and Sihvola [88, 89]. Indeed, the boundary condition $\mathbf{n} \cdot \mathbf{D} = 0$, which relates very closely to the principle of operation of the above structure for the TM fields, can be clearly separated from the conventional boundary condition $\mathbf{n} \times \mathbf{H}$ for magnetic conductors.

4.4.5 Numerical verification and comparison to the existing results

In [I]-[IV] and [1] the preceding analytical results were verified numerically and, when possible, compared to the existing results. In the following these results are reviewed shortly. The models for the different impedance surfaces are verified with full-wave simulations using commercial Ansoft's High Frequency Structure Simulator (HFSS) program [90]. The verification is done in terms of reflection phase diagrams. An application note describing the simulation model for such HFSS simulations can be found in [91]. For brevity, only structures composed of square patches are considered. First, the model for the artificial impedance surface (see (4.5)-(4.6)) is verified, after which the model for the mushroom structure ((4.6) and (4.13)) is considered. Finally, the models taking into account the spatial dispersion in the wire medium (4.15) and the additional varactor capacitances (4.18)-(4.19) are verified.

In [1] the analytical results were verified with an example of an artificial impedance surface with the following parameters (following the notations in Fig. 4.3): $a = b = 2\,$mm, $w = 0.1\,$mm, $h = 2\,$mm, and $\varepsilon_{\rm r} = 4$. The reflection phase results for the incidence angles of 0° and 60° degrees for both polarizations are shown in Fig. 4.7. The agreement between the analytical and simulation results is very good for both polarizations and all incidence angles. The analytical results for the artificial impedance surfaces were verified also in [I] with a number of simulations.

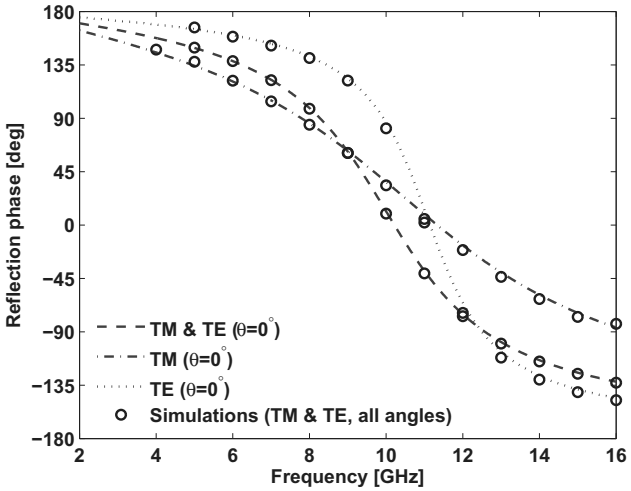

Figure 4.7: The reflection phase diagrams for the artificial impedance surface with the design parameters $a = b = 2\,\text{mm}$, $w = 0.1$ mm, $h = 2\,\text{mm}$, and $\varepsilon_\text{r} = 4$. The analytical results are calculated using (4.5) and (4.6) [1].

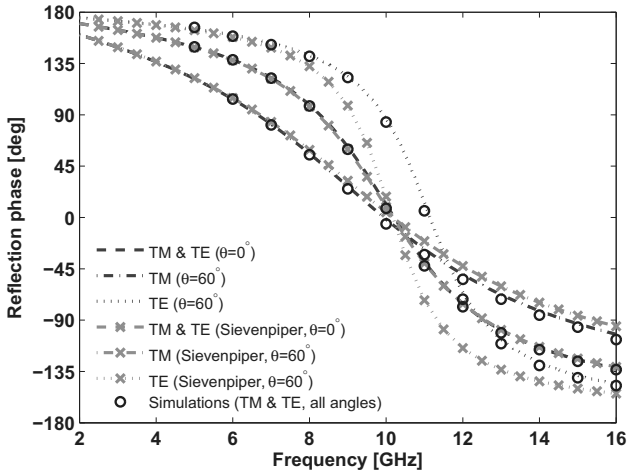

Figure 4.8: The reflection phase diagrams for the articial impedance surface with the design parameters $a = b = 2\,\text{mm}$, $w = 0.1$ mm, $h = 2\,\text{mm}$, $\varepsilon_\text{r} = 4$, and $r_0 = 0.05\,\text{mm}$. The analytical results are calculated using (4.6) and (4.13) [1]. Comparison is made also with the analytical model of Sievenpiper [78].

In the case of mushroom structures, the analytical verification of the analytical results were made in [II,III] and [1]. In [1] an example of the mushroom structure with the same design parameters as for the artificial impedance surface (see the reflection phase diagram in Fig. 4.7) were considered. The via radius was $r_0 = 0.05\,\text{mm}$. The reflection phase results for this structure calculated using (4.6) and (4.13) are compared with the model of Sievenpiper [78] and HFSS simulations in Fig. 4.8. Clearly, the model of Sievenpiper [78] becomes less accurate for the TE fields as the incidence angle grows. For the TM fields the accuracy of the Sievenpiper model remains rather good even for oblique incidence. The agreement between the simulation results and the analytical results calculated using (4.6) and (4.13) is very good for both polarizations and all incidence angles.

The results presented in Fig. 4.8 are for an electrically thin mushroom structure. When the electrical thickness of the structure increases, the assumption that the wire medium can be modeled as a uniaxial material fails. However, by taking the spatially dispersive properties of the wire medium into account, as is done in (4.15), this particular case can be modeled with very good accuracy. As an example of this, in [III] a mushroom structure was considered with the following design parameters: $a = b = 1\,\text{mm}$, $w = 0.1$ mm, $h = 5\,\text{mm}$, $\varepsilon_\text{r} = 1$, and $r_0 = 0.05\,\text{mm}$. The results according to the models (4.14) and (4.15) for TM fields are compared with the HFSS simulations in Fig. 4.9. It is clear from Fig. 4.9 that at low frequencies, when the mushroom structure is electrically thin, the

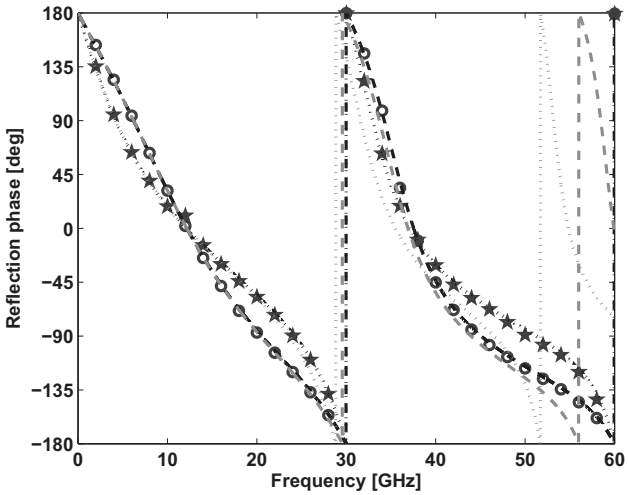

Figure 4.9: The reflection phase diagrams for the articial impedance surface with the design parameters $a = b = 1\,\text{mm}$, $w = 0.1$ mm, $h = 5\,\text{mm}$, $\varepsilon_\text{r} = 1$, and $r_0 = 0.05\,\text{mm}$. The results according to (4.15), (4.14), and simulations are in black, red, and blue, respectively. The simulation and the analytical results for the incidence angle $\theta = 30^\circ$ are plotted with circles and dashed lines, respectively. Similarly, the results for $\theta = 60^\circ$ are plotted with stars and dotted lines, respectively.

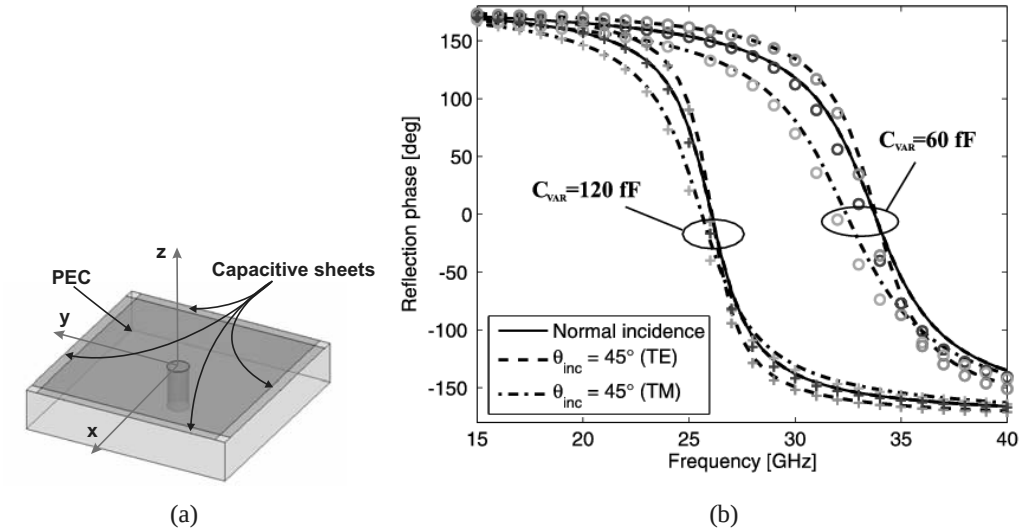

(a) (b)

Figure 4.10: (a) Simulation model of the tunable artificial impedance impedance surface unit cell. Because of the periodicity, the capacitance of each capacitive sheet equals to $2C_{\mathrm{var}}$. (b) The reflection phases for different angles of incidence and for different values of varactor capacitance. HFSS simulation results are denoted with crosses and circles for varactor capacitance values of 60 fF and 120 fF, respectively. The simulation results for normal incidence, 45° (TM), and 45° (TE) are colored blue, green, and red, respectively. The analytical results are plotted in black.

agreement with both of the analytical models and simulations is very good. However, as the electrical thickness of the mushroom structure grows at higher frequencies, the difference between the model (4.14) and the simulation results grows. The agreement between the model (4.15) and the simulation results remains good even for higher frequencies. Clearly, the effects of spatial dispersion become important for electrically thicker structures and cannot be neglected in the analytical models. However, in applications the preferable size of the artificial impedance surfaces is in general very thin.

Also, the plasma resonance of the wire medium can be used to achieve a resonance in the mushroom-like impedance surfaces. This can be done either far away from the main structural resonance of the impedance surface or close to it. The resonances predicted by the analytical formulas have been compared against the simulation results in [III,IV] (see also [VI]) and the results are in good agreement with each other.

Further, in [II] the model taking into account the additional varactor capacitances was verified numerically. In Fig. 4.10 (a) the simulation model of the varactor-tunable artificial impedance surface is shown. The reflection phases for the artificial impedance surfaces with the design parameters $a = b = 1\,\mathrm{mm}$, $w = 0.1\,\mathrm{mm}$, $h = 0.2\,\mathrm{mm}$, $\varepsilon_{\mathrm{r}} = 4$, and $r_0 =$

0.05 mm. The additional capacitance has the values of 60 pF and 120 pF. The analytically calculated and simulated reflection phase diagrams are shown in Fig. 4.10 (b) for the normal incidence and for the angle of $45°$. The agreement between the analytical results and the HFSS simulation results is good.

4.4.6 Experimental verification

In [V] the model for the artificial impedance surface without metallic vias embedded into the substrate has been verified experimentally with reflection phase measurements. The measurement setup is illustrated in Fig. 4.11. The measurements are done in an anechoic chamber. The sample under test is placed on a rotating unit that can be rotated remotely with an accuracy of $\pm 0.03°$. The sample is illuminated with the transmitting antenna. The distance between the transmitting antenna and the sample is approximately 5.3 m. The angle between the transmitting antenna and the surface of the sample is tuned to correspond to the correct angle of incidence, and the receiving antenna is then positioned with the help of mirrors and a laser. The laser is used to position and align the receiving antenna so that the laser beam launched from the transmitting antenna is reflected from the mirror on the sample to the mirror on the receiving antenna and all the way back to the laser. The distance between the receiving antenna and the sample is approximately 3.6 m.

The measurements were conducted for a sample with the following parameters: $a = b = 5.113$ mm, $w = 0.33$ mm, $h = 1.54$ mm, and $\varepsilon_{\mathrm{r}} = 4.4(1 - j0.02)$. The results of the measurements are compared also with the analytical models (4.5) and (4.6), and with simulation results obtained using HFSS. The measurement results are shown in Figs. 4.12 and 4.13 for TM and TE fields, respectively. The measurement result is the average and the standard deviation is given for every twentieth measurement point.

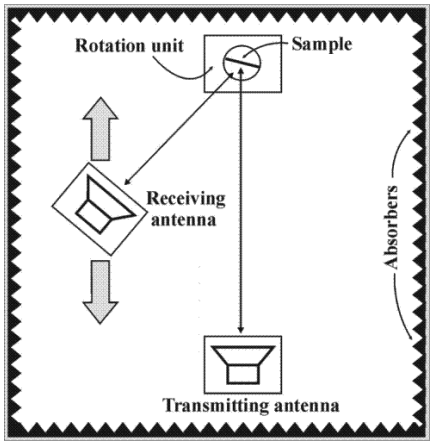

Figure 4.11: The measurement setup.

4.5 Summary of related publications

In [I] a simple and yet accurate analytical model has been derived for artificial impedance surfaces. The model is based on the analytical models derived for the capacitive screens in [I,II] and on the well-known model for a grounded dielectric slab. Compared to the existing models in the literature, the proposed model is strictly based on Maxwell's equations and is accurate even for oblique incidence. This is because most of the proposed models neglect the effects of spatial dispersion in the artificial impedance surface structure. In the proposed model the spatial dispersion is taken into account both in the grounded dielectric slab and in the capacitive screen lying over it. The model for the artificial impedance surface has been validated for different examples with numerical methods in [I].

In [II] the model for artificial impedance surfaces has been extended for mushroom-type structures by taking into account the effect of the vertical metallic vias. This is different from the model derived in [78] where the vias were neglected. The grounded dielectric slab embedded with metallic wires has been modeled as a wire medium slab with effective local material parameters (similarly as in [14, 51]), that is the spatial dispersion of the wire medium is assumed to be suppressed. Furthermore, the possibility to electrically tune the response of an artificial impedance surface with varactors has been studied. The effective averaged capacitance of the capacitive screen is mainly due to the small gaps between the adjacent metallic strips or patches. Therefore, a fair approximation can be made and the effective capacitance per unit cell can be written in a lumped element form

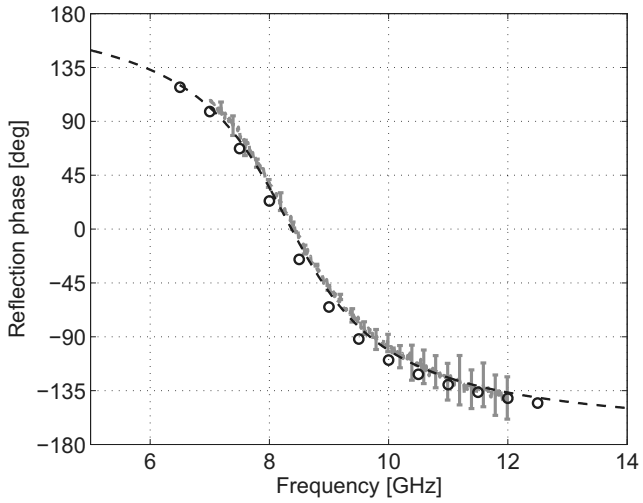

Figure 4.12: The reflection phase measurements at $\theta = 30^\circ$ for the TM fields. The solid red line corresponds to the measurement results, the dashed black line to the analytical results, and the black circles correspond to the HFSS simulation results.

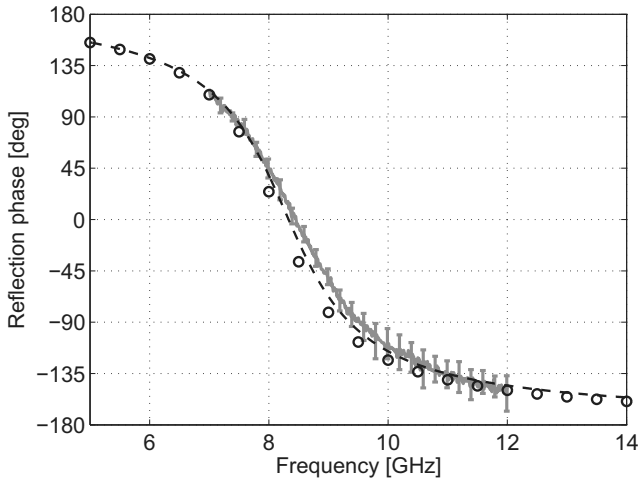

Figure 4.13: The reflection phase measurements at $\theta = 30^\circ$ for the TE fields. The solid red line corresponds to the measurement results, the dashed black line to the analytical results, and the black circles correspond to the HFSS simulation results.

for capacitors over the small gaps. This way the additional varactor capacitance can be easily taken into account through circuit theory formalism. The analytical model taking into account the additional capacitance of the varactors has been validated for different examples with numerical simulations in [II]. Compared to other models available in the literature, the proposed model shows good agreement with the simulation results even for oblique incidence.

The spatial dispersion of the wire medium in the context of the mushroom structure is studied more thoroughly in [III]. A model taking into account the spatial dispersion in the wire medium has been derived for the mushroom structure. In the models derived in [II], [51] (see also [IV,VI]) local material parameter values are used for the wire medium slab (the wire medium is considered to be spatially non-dispersive). However, the work of Silveirinha [73] clearly shows that a grounded wire medium slab may have properties very different from a uniaxial material slab with local material parameters. Also, in certain cases wire medium exhibits extreme anisotropy as shown by King [65], Tretyakov [14], and Silveirinha [73]. Although the arguments favoring the use of the local approximation of the permittivity of the wire medium are physically sound and the correctness of the assumption on the local material parameters in [II] have been numerically verified, there is an apparent contradiction with the studies of [70, 73]. As it turns out in [III], the studies [70, 73] and [II] are both correct. Namely, the effect of spatial dispersion in the wire medium can be nearly suppressed when the mushroom structure is electrically thin. Furthermore, the suppression of the spatial dispersion in the wire medium in the context of the mushroom structure leads to an additional resonance, as shown in [III].

This additional resonance of the mushroom structure occurs due to the plasma resonance of the wire medium.

The objective of [IV] has been to study possibilities to create all-angle artificial magnetic conductors with a stable response with respect to the incidence angle. The purpose has been to simplify the manufacturing of artificial magnetic conductors by using grounded uniaxial material slabs. It is thought that uniaxial symmetry allows one to renounce the structural isotropy, hence simplifying the manufacturing, without sacrificing the isotropy of the surface impedance. In order to achieve in this, the study has not been restricted only to naturally available materials.

The expression for surface the impedance of the grounded uniaxial material slab is derived for the local material parameters (no spatial dispersion). As a result of a systematical study, it is found that by using grounded uniaxial material slabs it is possible to achieve an all-angle magnetic-wall effect for both TE and TM polarization. For TM polarization a realizable structure is proposed and its performance is verified by simulations.

In [V] the analytical results of [I] have been verified experimentally. The measurement setup has been carefully described and reflection measurements are conducted on a sample for different angles of incidence. The reflection phase is calculated from these measurement results for different polarizations. The agreement between the analytical results calculated using the expressions in [I] and the measured reflection phases is good. This further verifies the results of [I].

5 Some applications based on artificial impedance surfaces

5.1 Introduction

Artificial impedance surfaces are not studied only for academic interest. The list of applications that utilize the exotic properties of artificial impedance surface cover electromagnetic band-gap structures (EBG) [92–95] and artificial magnetic conductors (AMC) [78, 96–99] for antenna applications, phase shifters and impedance waveguides [82, 100, 101], quasi-TEM waveguides [102–104], planar reflect-arrays [83, 84, 105, 106], and leaky-wave antennas [85, 86, 107] just to name a few. In the following, some applications are reviewed more thoroughly, namely electromagnetic absorbers, impedance waveguides, and electromagnetic band-gap structures.

5.2 Electromagnetic absorbers

5.2.1 Review of the literature and background

In electromagnetic absorbers the incident electromagnetic energy is dissipated into heat within the absorber structure. The electromagnetic energy can be coupled inside the absorber structure in many ways (see [108]). Here the discussion on the electromagnetic absorbers is constricted to resonant type of absorbers, which are electrically thin compared to the other type of absorber structures.

Classical structures for electromagnetic absorbers include Jaumann, Salisbury, and Dallenbach absorbers [109] (see also [16, 110]). The absorbers have been listed here in a chronological order, although the order of the first two absorbers named after their inventors is not evident. Apparently the Jaumann absorbers were used already during the second World War, whereas, to the best of the author's knowledge, there has been no mentioning in the literature that the Salisbury absorber would have been used already by this time. However, the patent for the Salisbury absorber was filed in 1952. For the Jaumann absorber the author has not found any such literature reference.

The difference between the Jaumann and Salisbury absorber can be easily understood by considering their principle of operation. In a Salisbury absorber losses are created with a resistive sheet that is placed at a distance of $\lambda/4$ over the ground plane, whereas in Jaumann absorbers resistive sheets are stacked over each other. The approximative distance of the resistive sheets in the Jaumann absorber is quarter wavelength (measured at the center frequency of the absorption band). By stacking the resistive sheets at an approximate quarter wavelength distance from each other, a number of closely positioned resonances can be created and a wider absorption band can be achieved compared to the Salisbury absorber. Actually, although the Jaumann and Salisbury absorbers have been invented

apparently at the same time, the Jaumann absorber can easily be considered to be a modification of the simpler Salisbury absorber. The principle of operation of both of them is the same. In contrast to the Jaumann and Salisbury absorbers, in Dallenbach absorber no resistive sheets are used. Instead, the incident power is dissipated in lossy homogenous dielectric materials layered on top of each other over a ground plane. Otherwise the Dallenbach absorber shares the similarities of the Jaumann and Salisbury absorbers.

In all the aforementioned absorbers the absorption mechanism relies on the quarter wavelength resonance of the grounded dielectric substrate. Depending on the application, the bandwidth of such an absorber may not be sufficient. One possibility to enlarge the absorption band is to use the same mechanism to create multiple resonances in the absorber, as is done in Jaumann absorber. Another possibility is to use different mechanism to create additional resonances in the vicinity of the primary, $\lambda/4$-wavelength, resonance of the grounded dielectric substrate. As an example, Reinert *et al.* [111] included chiral inclusions to the Dallenbach absorber's dielectric coatings and used the chiral resonance to enhance the absorption and enlarge the bandwidth of the absorber. Chandran *et al.* [112] used complex fractal geometries in a similar way. Further, in [113] Terracher *et al.* used a frequency selective surface (FSS) on top of a grounded dielectric substrate. All these absorption enhancement techniques widen the absorption band by creating an additional resonance in the vicinity of the $\lambda/4$-resonance. Because of this the electrical thickness of the structure remains still considerably large.

In order to reduce the electrical thickness of the structure, artificial impedance surfaces, or high-impedance surfaces, can be used for electromagnetic absorbers. This type of absorbers relate closely to the Salisbury absorber: The resonance is achieved by using the properties of the high-impedance surface and the absorption by a separate resistive sheet [114]. Also, one can incorporate the losses directly into the capacitive sheet over the grounded dielectric slab as was done by Kern *et al.* [115]. The resistive sheet can be realized by using commercially available resistive materials on top of the capacitive sheet or between the metallic parts of the capacitive sheet [116, 117]. One can even connect resistors between the adjacent metallic parts of the capacitive sheet of the high-impedance surface [118, 119]. The drawback of these designs, especially the ones using lumped resistors, is the inherent difficult way of realizing the resistive sheet (i.e. the high cost of high frequency lumped resistors and the number of spot welding).

Tretyakov *et al.* [120] proposed a simple way to realize the wanted absorption behavior in the artificial impedance surfaces: One simply needs to add losses to the grounded dielectric substrate. This method relates actually closely with the use of the resistive sheets. In electrically thin absorbers the amplitude of the electric fields is rather weak everywhere in the substrate except on the capacitive mesh (or rather between the adjacent patches). A part of the fringing electric fields between the patches exhibit the dielectric substrate that induces losses to the system. The losses can be therefore considered as a certain averaged sheet resistance acting on the surface current. Further, in [120] the stability with respect to the TM-polarized incidence angle was obtained by using metallic vias connecting the patches to the ground plane. The purpose was to use the extreme anisotropy of the wire medium formed by the metallic wires in the high-impedance surface favorably, and excite

only the TEM mode in the array of vias treated as the wire medium slab. Apart from this design topology, a similar approach as in [120] can be used to increase the absorption of resonant frequency selective surfaces in free space, as done in [121, 122].

5.2.2 Enlarging the operational band of resonant electromagnetic absorbers

In [VI] a novel technique to increase the absorption band of electromagnetic absorbers is proposed. The technique exploits an additional resonance for the TM-polarized oblique incidence in mushroom-like artificial impedance surfaces, when the plasma frequency of the wire medium slab is close to the original resonance of the artificial impedance surface. The analytical results are verified with numerical simulations done with CST Microwave Studio [123].

As an example, in [VI] an absorber based on a mushroom structure was considered with the following design parameters (following the notations of Fig. 4.5): $a = b = 10\,\text{mm}$, $w = 1.25\,\text{mm}$, $h = 3\,\text{mm}$, $\varepsilon_\text{r} = 2(1 - j0.5)$, and the radius of the wires was varied. The normalized plasma frequencies for the proposed structure and for the wire radii of $0.01\,\text{mm}$ and $0.1\,\text{mm}$ read, respectively, 3.6 GHz and 4.7 GHz. In Fig. 5.1 the power reflection factors are given for oblique incidence $\theta = 60^\circ$. The analytical results have been calculated using (4.5) and (4.6). In Fig. 5.1 (a) the power reflection factors are given for the TE fields. As expected, the metallic wires have practically no effect on the performance of the absorber for the TE polarization. For TM polarization the power reflection factors are shown in Fig. 5.1 (b). In addition to the structural resonance of the mushroom structure close to the plasma frequency also a plasma resonance of the wire medium is clearly seen in the results. For the wire radius of 0.01 mm the additional resonance lies reasonably far away from the primary structural artificial impedance surface resonance at approximately 7.5 GHz. For the wire radius of 0.1 mm the additional resonance is closer to the primary resonance and the absorption is enhanced considerably over the whole band.

The agreement between the analytical and simulation results is good. The results in Fig. 5.1 clearly show that by designing the plasma frequency of the wire medium close to the primary resonance of the artificial impedance surface, the absorption can be enhanced for the TM polarization. Evidently, the wires have no effect on the TE fields, which is a drawback of this technique. However, as the fields impinging on the absorber in practice are randomly polarized (excluding applications in which the absorbers are used in anechoic chambers), the proposed modification introduces an overall lowering of the reflected power.

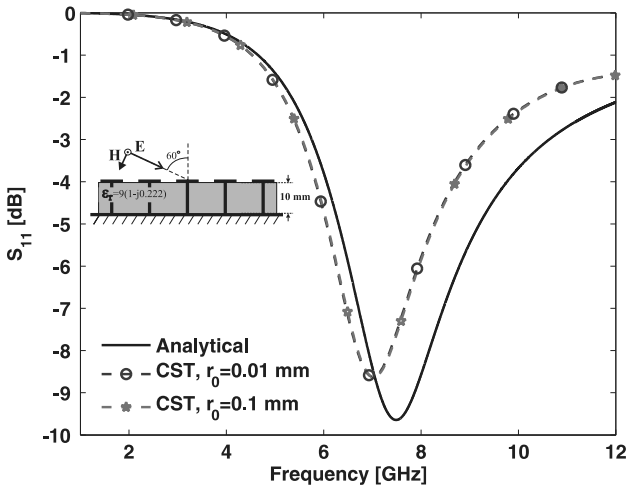

(a)

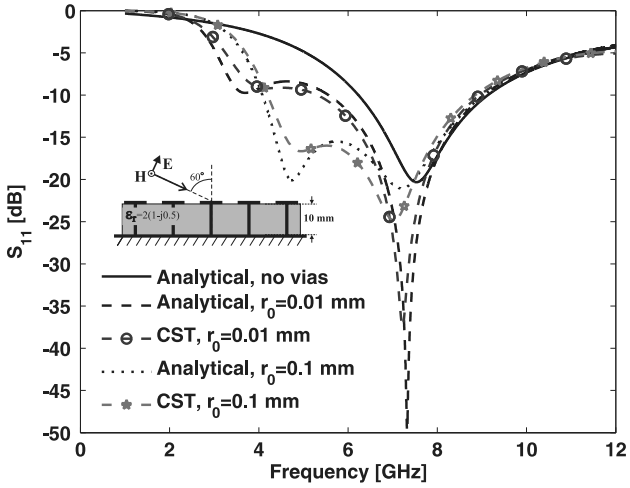

(b)

Figure 5.1: The effect of the vias to the power reflection factors for (a) TE and (b) TM polarization. The angle of incidence is $60°$. For the TE-polarized case the analytical results are the same for different via radii and in the absence of vias. The parameters of the absorber are the following: $a = b = 10\,\text{mm}$, $w = 1.25\,\text{mm}$, $h = 3\,\text{mm}$, and $\varepsilon_\text{r} = 2(1 - \text{j}0.5)$.

5.3 Impedance waveguides

5.3.1 Review of the literature and background

In impedance waveguides certain impedance boundaries are used as sidewalls of a waveguiding structure. Such impedance boundaries may be dielectric coated metal surfaces,

corrugated surfaces, or artificial impedance surfaces to name a few examples. Apparently the first analysis on the propagation properties of parallel-plate impedance waveguides have been made by Barlow [124] and Wait [125]. In 1965 Barlow [124] proposed initially to use the shielded impedance surfaces for surface waves that would be shielded from the surrounding environment. In [124] Barlow used corrugated surfaces to support TM-polarized surface waves. Later, in 1967, Wait [125] investigated the possibility to have also waveguide modes excited in the shielded surface wave guide and the contaminating effect of the waveguide modes to the initial surface wave mode suggested by Barlow. Barlow later found that the structure which he proposed supports also a quasi-TEM waveguide mode [126]. In [126, 127] also coaxial structures were considered. Later, in 1971, Dybdal [128] expanded the analysis to rectangular impedance waveguides. In a similar structure to an impedance waveguide, this type of waveguiding structures have been used in horn antennas for beam shaping [129–132]. Further, in waveguiding structures corrugated surfaces have been used to transform the fields inside the waveguides [133].

In corrugated surfaces, parallel slits are cut into a metal slab. At the frequency, where the corrugated surface appears as a magnetic wall for the TM fields, the electrical thickness of the corrugations equals to a quarter wavelength. The obvious drawback of the corrugated surfaces is that it can support only TM-polarized surface waves. For TE fields the corrugated surface appears as a metal surface. Therefore the above analyses have been restricted to TM fields. Also, due to the bulky structure of the corrugated surfaces, any tuning of the properties of the surface becomes unavoidably very difficult. Therefore, also other types of artificial impedance surfaces have been used in impedance waveguides. Artificial impedance surfaces composed of capacitive grids have the possibility to be easily tuned. For instance, Higgins and Xin *et al.* [82, 134] used this possibility to create an electrically tunable phase shifter with voltage tunable varactors. Later, the same principle was used in [101] with MEMS- (microelectromechanical systems) based tunable capacitors. Other than phase shifters, the impedance waveguides are used in stop-band [135] or band-pass [136] filters. In [82, 101, 134–136] the emphasis has been on proving the concept of the application rather than on the analysis of different modes in the waveguides. Also, only TE fields have been considered. More recently, Kehn *et al.* [137] have made analysis of dispersion in a rectangular waveguide with non-tunable impedance sidewalls numerically by using the method of moments.

5.3.2 Tunable impedance waveguides

In [II] the propagation properties of parallel-plate impedance waveguides are studied using the plane wave interpretation. In the plane wave interpretation the waveguide modes are considered to be formed by a set of plane waves with certain transverse and longitudinal wave numbers. To illustrate the problem, the geometry of a two-dimensional waveguide is shown in Fig. 5.2. The number of transverse wave vector components is limited to one as no propagation occurs in the x-direction. In the y-direction the waveguide has been confined by impedance surfaces $Z_{\mathrm{inp}}^{\pm}$. The superscript $\pm$ refers to the upper/lower surface, respectively. In Fig. 5.2 β is the propagation constant along the waveguide, k is the wave number, and k_{y} is the wave number in the y-direction, or the transverse wave

number. The dispersion relations for the structure can be solved from the boundary conditions at the impedance surface. The dispersion equations can be written for the TE and TM fields, respectively, as [II]

$$\tan(k_{\mathrm{y}}d) = j\eta\frac{k}{k_{\mathrm{y}}}\frac{Z^{+}_{\mathrm{inp}} + Z^{-}_{\mathrm{inp}}}{\eta^2\frac{k^2}{k_{\mathrm{y}}^2} + Z^{+}_{\mathrm{inp}}Z^{-}_{\mathrm{inp}}}, \tag{5.1}$$

$$\tan(k_{\mathrm{y}}d) = j\eta\frac{k_{\mathrm{y}}}{k}\frac{Z^{+}_{\mathrm{inp}} + Z^{-}_{\mathrm{inp}}}{\eta^2\frac{k_{\mathrm{y}}^2}{k^2} + Z^{+}_{\mathrm{inp}}Z^{-}_{\mathrm{inp}}}, \tag{5.2}$$

where η is the wave impedance in the medium filling the waveguide, d is the distance between the two impedance surfaces, and $k_{\mathrm{y}} = \pm\sqrt{k^2 - \beta^2}$ is the transverse wave number. By choosing the "minus"-branch of the transverse wave number, also surface modes on the waveguide sidewalls are predicted by the above dispersion equations. Actually, although the dispersion equations (5.1) and (5.2) are initially derived for a parallel-plate impedance waveguide having artificial impedance surfaces as sidewalls, they can be applied to more general cases. As a matter of fact, equations (5.1) and (5.2) are applicable for all cases where wave propagation between two impedance surfaces is studied, such as for surface waves in different structures. More recently, in 2009, similar results for the dispersion equations as presented here have been obtained independently by Holloway *et al.* [138].

As an example, in [II] a parallel-plate waveguide whose height was 7 mm was considered. In the Ka-band (26-40 GHz) only one waveguide mode would propagate in a metallic parallel-plate waveguide with the same dimension. Also, a case where the separation between the waveguide sidewalls is 3.5 mm was considered, so that the Ka-band lies below the cut-off. The waveguide was confined between identical mushroom surfaces composed of a capacitive mesh with the following design parameters: $a = b = 1$ mm, $g = 0.1$ mm, $h = 0.2$ mm, $\varepsilon_{\mathrm{r}} = 4$, and $r_0 = 0.05$ mm. In addition, a 60-pF capacitor was connected between the adjacent patches. The medium inside the impedance waveguide was air. In Figs. 5.3 and 5.4 the propagation properties in the 7-mm and 3.5-mm high waveguides, respectively, are illustrated. The analytical results show good agreement with the simulation results done with HFSS.

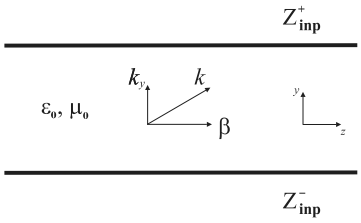

Figure 5.2: Illustration of the two-dimensional waveguide confined by two impedance surfaces.

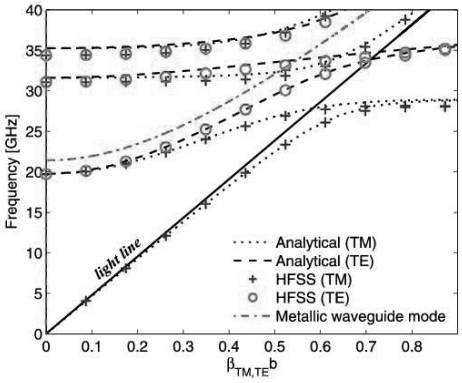

Figure 5.3: The propagation properties of a 7-mm high impedance waveguide with two tunable impedance surfaces. The value of the varactor capacitance is $C_{\mathrm{var}} = 60\,\mathrm{fF}$. The fundamental modes of the metal waveguide are plotted with dash-dot lines. β_{TE} and β_{TM} refer here to the propagation constants of the TE and TM modes, respectively.

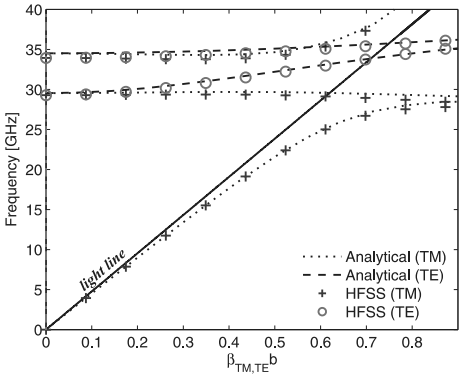

Figure 5.4: The propagation properties of a 3.5-mm below-cutoff impedance waveguide with two tunable impedance surfaces. The value of the varactor capacitance is $C_{\mathrm{var}} = 60\,\mathrm{fF}$. β_{TE} and β_{TM} refer here to the propagation constants of the TE and TM modes, respectively.

5.4 Electromagnetic band-gap structures in antenna applications

5.4.1 Review of the literature and background

Artificial impedance surfaces can be used also to suppress surface wave propagation. In this case for a given frequency band there exists no eigenvalue solution for surface waves.

For this reason this type of structures are also referred to as electromagnetic band-gap (EBG) structures with a close reference to photonic band-gap structures (PBG).

Corrugated surfaces, being a type of artificial impedance surface, have been widely studied in antenna applications since the 1950's and even earlier [57, 139–148]. Also EBG structures [149–153] and, more recently, artificial impedance surfaces studied in this thesis have been used in antenna applications [79, 92–95]. Here, attention is paid especially to the possibility to suppress surface waves on the impedance surface and this way enhance the radiation properties of the antenna. In finite-size metallic ground planes for antennas, the edges of the ground plane always influence the radiation pattern of the antenna due to the surface waves that reradiate from the edges. Further, the surface waves reduce the antenna efficiency by allowing energy to be coupled into bound modes traveling inside the surface structure rather than to propagating modes in free space. With an EBG surface these surface wave modes can be suppressed and a good radiation pattern can be restored.

Obviously, in order to succeed in this design, one should have knowledge on the dispersion behavior of the surface wave modes. This cannot be achieved analytically or even semi-analytically without an accurate model for the impedance surface. The dispersion of surface waves on a given artificial impedance surface can be solved by using the transverse resonance condition, as is done for instance in [18, 51, 154, 155]. In [51] the dispersion properties of artificial impedance surfaces were studied semi-analytically. This means that the closed-form expressions for the surface impedance were functions of the transverse wave number. Therefore the dispersion equations resulting from the transverse resonance condition needed to be solved numerically. Naturally, approximations on the properties of the artificial impedance surfaces can be made in order to write the surface impedance in a non-spatially dispersive form and facilitate the calculation of dispersion properties of the surface waves on these surfaces. Such approximations can be done, for instance, for artificial impedance surfaces comprising high-ε_{r} substrates or relatively high, densely packed wire medium slabs (the extreme anisotropy in the wire medium). No verification of the results were given in [51].

5.4.2 Analysis of the surface waves

In [VII] a comparison of the dispersion properties of the surface waves on an artificial impedance surface without metallic vias and on a mushroom surface was made. As an example, the following design parameters for the surfaces were considered in [VII] (following the notations in Fig. (4.3) and (4.5)): $a = b = 2\,\mathrm{mm}$, $h = 1\,\mathrm{mm}$, $w = 0.2\,\mathrm{mm}$, $\varepsilon_{\mathrm{r}} = 10.2$, and when applicable $r_0 = 0.05\,\mathrm{mm}$. In Figs. 5.5 and 5.6 the dispersion behavior of the surface waves for the artificial impedance surface and for the mushroom surface are shown, respectively. The results have been verified with HFSS simulations. The proper modes refer to the physical solutions of the transverse resonance condition whereas the improper ones refer to the nonphysical solutions satisfying the same condition. Both solutions are obtained from different branches of the same dispersion equation.

It is shown in Figs. 5.5-5.6 and in [VII] that for the surface structure without wires there exists no band gap, whereas for the surface structure with vias there exists one. Furthermore, for the TM surface waves on the artificial impedance surface with wires there exists a backward-wave solution predicted also by the analytical model.

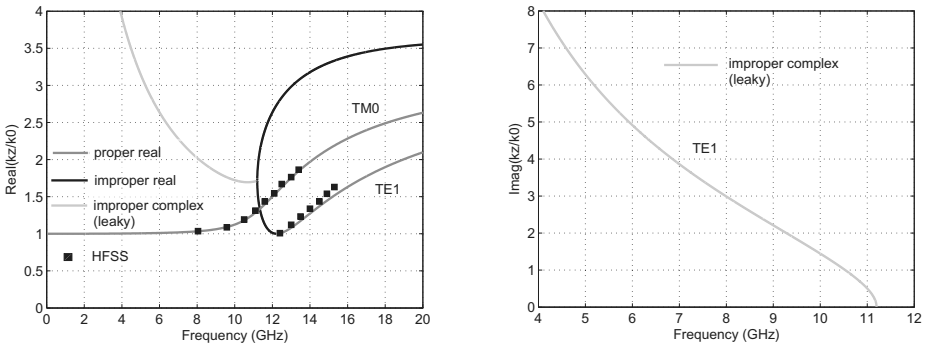

(a) (b)

Figure 5.5: Dispersion behavior of surface waves on the HIS without vias. (a) The real part of the normalized propagation constant. (b) The imaginary part of the normalized propagation constant.

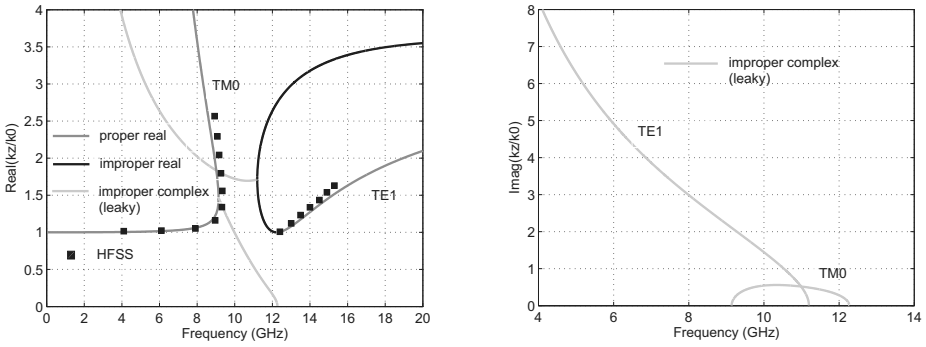

(a) (b)

Figure 5.6: Dispersion behavior of surface waves on the HIS with vias. (a) The real part of the normalized propagation constant. (b) The imaginary part of the normalized propagation constant.

5.5 Summary of related publications

In [VI] a new type of technique to enlarge the absorption band of a resonant-type absorber is introduced. The technique is based on the use of the plasma resonance of wire medium in the context of mushroom structure (see [III]). When the plasma resonance of the wire medium is designed close to the main structural resonance of the mushroom-type artificial impedance surface, the total absorption of the structure is enhanced and the operational bandwidth enlarged. As long as the wire medium is excited by the incident fields, the plasma resonance is independent from the incidence angle.

In [II] a semi-analytical model is derived for calculating the propagation constants in an impedance waveguide. In the derivations it is assumed that the different modes in the waveguide consist of a set of plane waves, for which the response at the boundaries of the waveguide is well known from our previous works. This model is used to study the propagation properties in different tunable impedance waveguides. Depending on the size of the waveguide different phenomena are found in tunable impedance waveguides. In an oversized waveguide it is possible to convert one mode to another. In a single-mode waveguide one can have multi-mode propagation and band gaps. Also, forward- as well as backward-wave propagation can occur in a below-cutoff waveguide.

Finally, in [VII] a comparative study on the propagation properties of surface waves on different type of artificial impedance surfaces is made. The objective of the study has been to verify that the analytical expressions for the surface impedance of different types of artificial impedance surfaces can be used to calculated the propagation properties of surface waves.

6 Conclusions

In this thesis several types of grids, artificial impedance surfaces, and mushroom structures have been studied. Emphasis has been on the analytical modeling of these structures. These surfaces posses many features that can be exploited in different applications in radio engineering.

First, capacitive grids and meshes have been studied. An averaged boundary condition for the oblique incidence has been derived for these structures starting from the boundary conditions for their complementary structures and using the approximate Babinet's principle. The resulting boundary conditions are applicable not only for screens in homogeneous materials, but also for screens at an interface of two media. Comparison with the existing results found in the literature as well as with numerical results has been made. The derived boundary conditions for capacitive grids show good agreement with the results found in the literature. For capacitive meshes, the derived boundary conditions show better agreement with the numerical results than the existing solutions.

Secondly, the averaged boundary conditions for capacitive screens have been used to derive accurate boundary conditions for artificial impedance surfaces. Further, the effect of wire medium composed of vertical metallic wires in the substrate of mushroom-like impedance surfaces has been taken into account in the boundary conditions as well as the effect of additional capacitances between the adjacent metallic patches or strips. The effect that the spatial dispersion of the wire medium has on the characteristics of the mushroom structures has been studied in detail. In the cases when the mushroom structure is electrically thin or when the wire medium is characterized with extreme anisotropy, a local model can be used to characterize the properties of the wire medium in the mushroom structure topology. It is found that in the case when the spatial dispersion in the wire medium is suppressed, an additional resonance is created in the vicinity of the main resonance of the mushroom structure due to the plasma resonance of the wire medium. The developed boundary conditions for artificial impedance surfaces and mushroom structures have been verified in their region on validity using various numerical methods. Also, the analytical results have been experimentally verified. Compared to other existing analytical solutions, the present results show better agreement with the numerical results.

Further, the properties of grounded uniaxial material slabs have been studied analytically. The results show that it is possible to create an isotropic magnetic wall effect in the surface plane (*cf.* AMC). This new design simplifies the manufacturing of the AMC planes considerably. In the most promising case the magnetic wall effect can be realized for the TM fields by having $\varepsilon_{\mathrm{n}} \to 0$. As an example, it has been shown that this type of surface can be realized using wire medium at its plasma frequency and suppressing the spatial dispersion of the wire medium. The analytical results have been verified numerically.

Finally, the studied mushroom structures have been applied to selected radio engineering applications. These applications are the electromagnetic absorbers, impedance waveguides, and electromagnetic band-gap structures. In electromagnetic absorbers, the ab-

sorption band of the absorbers is enlarged and the absorption is enhanced by using the additional resonance in the mushroom structure. Although the additional resonance occurs only for the TM fields, in practice waves impinging on the surface have random polarization. Because of this, the proposed modification introduces an average lowering in the reflected power in such applications, for instance, that aim to reduce the radar cross section of an object. The analytical results have been verified with numerical simulations and the agreement between the results is shown to be good.

In impedance waveguides, the possibility to tune the resonance frequency of the mushroom structures has been used to create tunable impedance waveguides. An analytical model for the dispersion properties of waves in a parallel-plate waveguide has been derived. Actually, in its generality, the model can be used to model waves in any environment confined with two impedance boundaries. The model is used to study the propagation properties in the impedance waveguide. In waveguides of electrically small height multi-mode propagation and band gaps are shown. Furthermore, forward- as well as backward-wave propagation in a below-cutoff waveguide is presented. The results are verified with numerical simulations.

In the case of electromagnetic band-gap structures, comparison between the dispersion properties of artificial impedance surfaces and mushroom-structures is made semi-analytically and numerically. Evidently, the dispersion properties of these surfaces are very different for the TM surface waves. Moreover, the preceding analytical models for these surfaces are verified to be accurate even for modeling of surface waves.

References

[1] O. Luukkonen, C. R. Simovski, and S. A. Tretyakov, "Microwave devices based on tunable metasurfaces," *Proc. of the 37th European Microwave Conference, Munich, Germany,* 8–12 October 2007, pp. 489–492.

[2] O. Luukkonen, M. G. Silveirinha, A. B. Yakovlev, C. R. Simovski, I. S. Nefedov, and S. A. Tretyakov, "Homogenization models for the analysis of reflection properties of mushroom structures," *Proc. 2nd International Congress on Advanced Electromagnetic Materials in Microwaves and Optics, Pamplona, Spain*, September 21–26, 2008, pp. 208–210.

[3] A. B. Yakovlev, M. G. Silveirinha, O. Luukkonen, C. R. Simovski, I. S. Nefedov, and S. A. Tretyakov, "Homogenization models for the analysis of surface waves on mushroom structures," *Proc. 2nd International Congress on Advanced Electromagnetic Materials in Microwaves and Optics, Pamplona, Spain*, September 21–26, 2008, pp. 310–312.

[4] O. Luukkonen, C. Simovski, and S. Tretyakov, "Beam-steering with a high-impedance surface", *13th International Student Seminar on Microwave Applications of Novel Physical Phenomena*, Rovaniemi 24–25 August, 2006, pp. 33–35.

[5] O. Luukkonen, C. Simovski, A. V. Räisänen, and S. A. Tretyakov, "Analysis of varactor-tunable high-impedance surfaces and waveguides," *Proc. PIERS 2008, Hangzhou, China*, 24–28 March, 2008, p. 456.

[6] A. V. Räisänen, J. Ala-Laurinaho, D. Chicherin, S. Dudorov, A. Karttunen, D. Lioubtchenko, O. Luukkonen, J. Mallat, P. Pousi, A. Tamminen, M. Vaaja, "Mm- and submm-wave research activities at MilliLab and SMARAD," *Proc. of Global Symposium on Millimeter Waves*, 21–24 April, 2008, pp. 136–137.

[7] A. B. Yakovlev, C. R. Simovski, S. A. Tretyakov, O. Luukkonen, G. W. Hanson, S. Paulotto, and P. Baccarelli, "Analytical modeling of surface waves on high impedance surfaces," *Proc. Meta'08, NATO Advanced Research Workshop, Marrakesh, Morocco*, 7-10 May, 2008, pp. 184–193.

[8] O. Luukkonen, F. Costa, A. Monorchio, and S. A. Tretyakov, "Increasing the absorption band of thin electromagnetic absorbers by using plasma resonance of wire medium," *2009 IEEE AP-S International Symposium on Antennas and Propagation, Charleston*, South Carolina, USA, June 01-05, 2009, paper s423p2.

[9] O. Luukkonen, C. R. Simovski, and S. A. Tretyakov, "Magnetic conductor based on uniaxial materials with extreme material parameters," *2009 IEEE AP-S International Symposium on Antennas and Propagation, Charleston*, South Carolina, USA, June 01-05, 2009, paper s123p2.

[10] A. B. Yakovlev, O. Luukkonen, C. R. Simovski, S. A. Tretyakov, S. Paulotto, P. Baccarelli, and G. W. Hanson, "Analytical modeling of surface waves on high impedance surfaces,"*Metamaterials and Plasmonics: Fundamentals, Modelling, Applications* (Eds. S. Zouhdi, A. Sihvola, and A. P. Vinogradov), NATO Science for Peace and Security Series B, pp. 239–254, 2009.

[11] A. B. Yakovlev, M. G. Silveirinha, O. Luukkonen, C. R. Simovski, I. S. Nefedov, and S. A. Tretyakov, "Homogenization models for the characterization of surface-wave propagation on mushroom structures," *IEEE Trans. Microwave Theory Tech.*, vol. 57, no. 11, pp. 2700-2714, Nov. 2009.

[12] T. B. A. Senior and J. L. Volakis, *Approximate Boundary Conditions in Electromagnetics*, London: IEE Electromagnetic Waves Series, 1995.

[13] D. J. Hoppe and Y. Rahmat-Samii, *Impedance Boundary Conditions in Electromagnetics*, Washington, D.C.: Taylor and Francis, 1995.

[14] S. A. Tretyakov, *Analytical Modeling in Applied Electromagnetics*, Norwood, MA: Artech House, 2003.

[15] C. C. Chen, "Transmission through a conductiong screen perforated periodically with apertures," *IEEE Trans. Microwave Theory Tech.*, vol. MTT-18, pp. 627–632, 1970.

[16] B. A. Munk, *Frequency Selective Surfaces: Theory and Design.* New York: Wiley, 2000.

[17] K. W. Whites and R. Mittra, "An equivalent boundary-condition for lossy periodic structures at low frequencies," *IEEE Trans. Antennas Propag.*, vol. 44, no. 12, pp. 1617–1629, Dec. 1996.

[18] S. Maci, M. Caiazzo, A. Cucini, and M. Casaletti, "A pole-zero mathcing method for EBG surfaces composed of a dipole FSS printed on a grounded dielectirc slab," *IEEE Trans. Antennas Propag.*, vol. 53, no. 1, pp. 70–81, Jan. 2005.

[19] R. T. Compton and R. E. Collin, "Slot antennas," in *Antenna Theory*, (Eds. R. E. Collin and F. J. Zucker), McGraw-Hill: New York, 1969, pp. 560–616.

[20] H. Lamb, "On the reflection and transmission of electric waves by a metallic grating," *Proc. London Math. Soc.*, Ser. 1, vol. 29, pp. 523–544, 1898.

[21] W. von Ignatowsky, "Theory of the grating," *Ann. der Phys.*, vol. 44, pp. 369–436, May 1914.

[22] M. I. Kontorovich, "Screening properties of a closed grid," [Russian] *Zh. Tekh. Fiz.*, vol. 9, pp. 2195–2210, 1939.

[23] G. G. MacFarlane, "Surface impedance of an infinite wire grid, at oblique angles of incidence," *J. IEE*, vol. 93 (III E), pp. 1523–1527, Dec. 1946.

[24] W. Wessel, "On the passage of electromagnetic waves through a wire grid," *Hochfrequenztechnik,* vol. 54, pp. 62–69, Jan. 1939.

[25] R. Hornejäger, "Electromagnetic properties of wire grids," *Ann. der Physik*, vol. 4, pp. 25–35, Jan. 1948.

[26] J. R. Wait, "Reflection at arbitrary incidence from a parallel wire grid," *Appl. Sci. Research*, vol. B4, pp. 393–400, 1955.

[27] E. A. Lewis and J. Casey, "Electromagnetic reflection and transmission by a grating of resistive wires," *J. Appl. Phys.*, vol. 23, pp. 605–606, June 1952.

[28] G. von Trentini, "Gratings as circuit elements of electric waves in space," *Zeit. angew. Phys.*, vol. 5, pp. 221–231, June 1953.

[29] N. Marcuvitz (ed.), *Waveguide Handbook*, IEE Electromagnetic Waves Series 21, McGraw-Hill: New York, 1951.

[30] J. R. Wait, "The impedance of wire grid parallel to a dielectric interface," *IRE Trans. Microwave Theory Tech.*, vol. MTT-5, no. 2, pp. 99–102, April 1957.

[31] J. Young and J. R. Wait, "Note on the impedance of a wire grid parallel to a homogeneous interface," *IEEE Trans. Microwave Theory Tech.*, vol. 37, no. 7, pp. 1136–1138, July 1989.

[32] T. Sakurai, "Electromagnetic phenomena on ribbon elements grating," *J. Phys. Soc. Japan*, vol. 5, pp. 203–207, 1950.

[33] A. N. Sivov, "Electrodynamic theory on a dense plane grating of parallel conductors," [Russian] *Radiotekh. Elektron.*, vol. 6, pp. 483–495, 1961 [English transl. in *Radio Eng. Electron. Phys.*, vol. 6, pp. 429–440, 1961].

[34] L. A . Wainstein, "On the electrodynamic theory of grids," [Russian] in *Elektronika Bol'shikh Moshchnostein*, vol. 2 (Eds. P. L. Kapitsa and L. A. Wainstein), Nauka, Moscow, 1963 [English transl. in *High-power Electronics*, Pergamon Press, Oxford, pp. 14–48, 1966].

[35] A. I. Adonina and V. V. Shcerbak, "Equivalent boudanry conditions at a metal grating situated between two magnetic materials," [Russian] *Zh. Tekh. Fiz.* vol. 34, pp. 333–335, 1964 [English transl. in *Sov. Phys. Tech. Phys.* vol. 9, pp. 261–263, 1964].

[36] S. Ye. Bankov and I. V. Levchenko, "Equivalent boundary conditions for a closely spaced ribbon grating at the interface of two media," [Russian] *Radiotekh. Elektron.*, vol. 33, pp. 2045–2050, 1988 [English transl. in *Sov. J. Commun. Technol. Electron.*, vol. 34, no. 5, pp. 67–72, 1989].

[37] R. R. DeLyser and E. F. Kuester, "Homogenization analysis of electromagnetic strip gratings," *J. of Electromagn. Waves and Appl.*, vol. 5, no. 11, pp. 1217–1236, 1991.

[38] M. I. Kontorovich, V. Y. Petrunkin, N. A. Yesepkina, and M. I. Astrakhan, "The coefficient of reflection of a plane electromagnetic wave from a plane wire mesh," *Radio Eng. Electron Phys.*, no. 7, pp. 222–231, 1962.

[39] M. I. Astrakhan, "Averaged boundary conditions on the surface of a lattice with rectangular cells," *Radio Eng. Electron Phys.*, no. 9, pp. 1239–1241, 1964.

[40] R. Ulrich, K . F. Renk, and L. Genzel, "Tunable submillimeter interferometers of the Fabry-Perot type," *IEEE Trans. Microwave Theory Tech.*, vol. 11, no. 5, pp. 363–371, 1963.

[41] D. A. Hill and J. R. Wait, "Analyses of electromagnetic scattering from wire-mesh structures," *Electron. Lett.*, vol. 12, no. 17, Aug. 1976.

[42] S.-W. Lee, G. Zarrillo, and C.-L. Law, "Simple formulas for transmission through periodic metal grids or plates," *IEEE Trans. Antennas Propag.*, vol. AP-30, no. 5, pp. 904–909, 1982.

[43] V. V. Yatsenko, S. A. Tretyakov, S. I. Maslovski, and A. A. Sochava, "Higher order impedance boundary conditions for sparse wire grids," *IEEE Trans. Antennas Propag.*, vol. 48, no. 5, pp. 720–727, 2000.

[44] R. Ulrich, "Far-infrared properties of metallic mesh and its complementary structure," *Infrared Phys.*, vol. 7, no. 1, pp. 37–50, 1967.

[45] T. Timusk and P. L. Richards, " Near millimeter wave bandpass filters," *Appl. Opt.*, vol. 20, no. 8, pp. 1355–1359, 1981.

[46] S. T. Shanahan and N. R. Heckenberg, "Transmission line model of substrate effects on capacitive mesh couplers," *Appl. Opt.*, vol. 20, no. 23, pp. 4019–4023, 1981.

[47] R. C. Compton, L. B. Whitbourn, and R. C. McPherdan, "Strip gratings at a dielectric interface and application of Babinet's principle," *Appl. Opt.*, vol. 23, no. 18, pp. 3236–3242, Sep. 1984.

[48] L. B. Whitbourn and R. C. Compton, "Equivalent-circuit formulas for metal grid reflectors at a dielectric boundary," *Appl. Opt.*, vol. 24, no. 2, pp. 217–220, 1985.

[49] C. L. Holloway, M. A. Mohammed, and E. F. Kuester, "Reflection and transmission properties of a metafilm: With an application to a controllable surface composed of resonant particles," *IEEE Trans. Electromagn. Compat.*, vol. 47, no. 4, pp. 853–865, 2005.

[50] E. F. Kuester, M. A. Mohammed, M. Piket-May, and C. L. Holloway, "Averaged transition conditions for electromagnetic fields at a metafilm," *IEEE Trans. Antennas Propag.*, vol. 51, no. 10, pp. 2641–2651, 2003.

[51] S. Clavijo, R. E. Díaz, and W. E. McKinzie, III, "High-impedance surfaces: An artificial magnetic conductor for a positive gain electrically small antennas," *IEEE Trans. Antennas Propagat.*, vol. 51, no. 10, pp. 2678–2690, 2003.

[52] G. Granet and J.-P. Plumey, "Parametric formulation of the Fourier modal method for crossed surface-relief gratings," *J. Opt. A*, vol. 4, no. 5, pp. S145–S149, 2002.

[53] G. Granet and B. Guizal, "Analysis of strip gratings using a parametric modal method by Fourier expansions," *Opt. Commun.*, vol. 255, no. 1–3, pp. 1–11, 2005.

[54] R. Elliot, "On the theory of corrugated plane surfaces," *IRE Trans. Antennas Propagat.* , vol. 2, pp. 71–81, Apr. 1954.

[55] S. Lee and W. Jones, "Surface waves on two-dimensional corrugated surfaces," *Radio Sci.*, vol. 6, pp. 811–818, 1971.

[56] Y.-L. Chen and Y. Lo, "Reactive reflectors," *Proc. Inst. Elect. Eng.*, pt. H, vol. 131, pp. 263–269, 1984.

[57] P.-S. Kildal, "Artificially soft and hard surfaces in electromagnetics," *IEEE Trans. Antennas Propagat.*, vol. 38, pp. 1537–1544, Oct. 1990.

[58] J. Brown, "Artificial dielectrics having refractive indices less than unity," *Proc. IEE*, Monograph no. 62R, vol. 100, pt. 4, pp. 51–62, May 1953.

[59] J. Brown and W. Jackson, "The properties of artificial dielectrics at centimeter wavelengths," *Proc. IEE*, paper no. 1699R, vol. 102B, pp. 11–21, Jan. 1955.

[60] A. Carne and J. Brown, "Theory of reflections from the rodded-type artificial dielectric," *Proc. IEE*, paper no. 2742R, vol. 105C, pp. 107–115, Nov. 1958.

[61] J. S. Seeley and J. Brown, "The use of dispersive artificial dielectrics in a beam scanning prism," *Proc. IEE*, paper no. 2735R, vol. 105C, pp. 93–102, Nov. 1955.

[62] J. Brown, "Artificial dielectrics," in *Progress in dielectrics*, (Eds. J. B. Birks and J. H. Schulman), vol. 2, pp. 195–225, 1960.

[63] W. Rotman, "Plasma simulation by artificial dielectrics and parallel plate media," *IRE Trans. Antennas Propagat.*, vol. 10, pp. 82–95, 1962

[64] A. Sihvola, *Electromagnetic Mixing Formulas and Applications*, Inst. Elect. Eng. Electromagnetic Waves Series 47. London, U.K, 1999.

[65] R. J. King, D. V. Thiel, and K. S. Park, "The synthesis of surface reactance using an artificial dielectric," *IEEE Trans. Antennas Propag.*, vol. 31, no. 3, pp. 471–476, May 1983.

[66] A. F. Kay, " Applied problems in electromagnetic theory," Tech. Res. Group, contract AF 19(604)-3476, AD 261 286, Apr. 1961.

[67] H. B. Querido, in C. H. Walter, *Travelling Wave Antennas.* McGraw-Hill: New York, 1965.

[68] C. A. Moses and N. Engheta, "Electromagnetic wave propagation in the wire medium: a complex medium with long thin inclusions," *Wave Motion*, vol. 34, no. 3, pp. 301–317, Sep. 2001.

[69] P. Belov, S. A. Tretyakov, and A. J. Viitanen, "Dispersion and reflection properties of artificial media formed by regular lattices of ideally conducting wires," *J. of Electromagn. Waves and Appl.*, vol. 18, no. 8, pp. 1153–1170, 2002.

[70] P. A. Belov, R. Marqués, S. I. Maslovski, I. S. Nefedov, M. Silveirinha, C. R. Simovski, and S. A. Tretyakov, "Strong spatial dispersion in wire media in the very large wavelength limit," *Phys. Rev. B*, vol. 67, 113103, 2003.

[71] M. Silveirinha, "Additional boundary condition for the wire medium," *IEEE Trans. Antennas Propag.*, vol. 54, p. 1766, 2006.

[72] M. G. Silveirinha, C. A. Fernandes, and J. R. Costa, "Additional boundary condition for a wire medium connected to a metallic surface," *New J. Phys.*, vol. 10, 053011, 2008.

[73] M. G. Silveirinha, C. A. Fernandes, and J. R. Costa, "Electromagnetic characterization of textured surfaces formed by metallic pins," *IEEE Trans. Antennas Propag.*, vol. 56, no. 2, pp. 405–415, Feb. 2008.

[74] A. Demetriadou and J. Pendry, "Taming spatial dispersion in wire metamaterial," *J. Phys.: Condens. Matter*, vol. 20, 295222, 2008.

[75] C.-C. Liu, J. Shmoys, A. Hessel, J. D. Hanfling, and J. M. Usoff, "Plane wave reflection from microstrip-patch arrays - theory and experiment," *IEEE Trans. Antennas Propag.*, vol. AP-33, no. 4, pp. 426–435, 1985.

[76] K.-P. Ma, K. Hirose, F.-R. Yang, Y. Qian, and T. Itoh, "Realization of magnetic conducting surface using novel photonic bandgap structure," *Electron. Lett.*, vol. 34, no. 21, pp. 2041–2042, Oct. 1998.

[77] F.-R. Yang, K.-P. Ma, Y. Qian, and T. Itoh, "A novel TEM waveguide using uniplanar compact photonic-bandgap (UC-PBG) structure," *IEEE Trans. Microwave Theory Tech.*, vol. 47, no. 11, pp. 2092–2098, Nov. 1999.

[78] D. Sievenpiper, "High-impedance electromagnetic surfaces," Ph.D. Dissertation, Univ. California, Dept. Elect. Eng., Los Angeles, CA, 1999.

[79] D. Sievenpiper, L. Zhang, R. F. J. Broas, N. G. Alexopoulos, and E. Yablonovich, "High-impedance electromagnetic surfaces with a forbidden frequency band," *IEEE Trans. Microwave Theory Tech.*, vol. 47, no. 11, pp. 2059–2074, Nov. 1999.

[80] S. A. Tretyakov and S. I. Maslovski, "Thin absorbing structure for all incident angles based on the use of a high-impedance surface," *Microw. Opt. Tech. Lett.*, vol. 38, no. 3, pp. 175–178, 2003.

[81] S. A. Tretyakov and C. R. Simovski, "Dynamic model of artificial reactive impedance surfaces," *J. of Electromagn. Waves and Appl.*, vol. 17, no. 1, pp. 131–145, 2003.

[82] J. A. Higgins, H. Xin, A. Sailer, and M. Rosker, "Ka-band waveguide phase shifter using tunable electromagnetic crystal sidewalls," *IEEE Trans. Microwave Theory Tech.*, vol. 51, no. 4, pp. 1281–1287, April 2003.

[83] D. Sievenpiper, J. Schaffner, R. Loo, G. Tangonan, S. Ontiveros, and R. Harold, "A tunable impedance surface performing as a reconfigurable beam steering reflector," *IEEE Trans. Antennas Propag.*, vol. 50, no. 3, pp. 384–390, Mar. 2002.

[84] D. Sievenpiper and J. Schaffner, "Beam steering microwave reflector based on electrically tunable impedance surface," *Electron. Lett.*, vol. 38, no. 21, pp. 1237–1238, Oct. 2002.

[85] D. Sievenpiper, J. Schaffner, J. J. Lee, S. Livingston, "A steerable leaky-wave antenna using a tunable impedance ground plane," *IEEE Antennas Wireless Propag. Lett.*, vol. 1, pp. 179–182, 2002.

[86] D. F. Sievenpiper, "Forward and backward leaky wave radiation with large effective aperture from an electronically tunable textured surface," *IEEE Trans. Antennas Propag.*, vol. 53, no. 1, pp. 236–247, Jan. 2005.

[87] C. Mias and J. H. Yap, "A varactor-tunable high impedance surface with a resistive-lumped-element biasing grid," *IEEE Trans. Antennas Propag.*, vol. 55, no. 7, pp. 1955–1962, July 2007.

[88] I. V. Lindell and A. H. Sihvola, "Electromagnetic boundary and its realization with anisotropic metamaterial," *Phys. Rev. E*, vol. 79, 026604, 2009.

[89] I. V. Lindell and A. H. Sihvola, "Uniaxial IB-medium interface and novel boundary conditions," *IEEE Trans. Antennas Propag.*, vol. 57, no. 3, pp. 694-700, 2009.

[90] Ansoft's homepage: http://www.ansoft.com/

[91] Application note "ANALYSIS OF PHOTONIC BANDGAP SURFACES USING ANSOFT HFSS" on how to calculate the reflection phase from an infinitely large high-impedance surface: http://www.ansoft.com/news/articles/analysis_of_photonic_bandgap_surfaces.pdf

[92] R. Gonzalo, P. De Maagt, and M. Sorolla, "Enhanced patch-antenna performance by suppressing surface waves using photonic-bandgap substrates," *IEEE Trans. Microwave Theory Tech.*, vol. 47, no. 11, pp. 2131-2138, Nov. 1999.

[93] F. Yang, and Y. Rahmat-Samii, "Microstrip antennas integrated with electromagnetic band-gap (EBG) structures: a low mutual coupling design for array applications," *IEEE Trans. Antennas Propag.*, vol. 51, no. 10, pp. 2936–2946, Oct. 2003.

[94] R. F. J. Broas, D. F. Sievenpiper, and E. Yablonovitch, "An application of high-impedance ground planes to phased array antennas," *IEEE Trans. Microwave Theory Tech.*, vol. 53, no. 4, pp. 1377–1381, April 2005.

[95] R. Baggen, M. Martinez-Vazquez, J. Leiss, S. Holzwarth, L. S. Drioli, and P. de Maagt, "Low profile GALILEO antenna using EBG technology," *IEEE Trans. Antennas Propag.*, vol. 56, no. 3, pp. 667–674, March 2008.

[96] D. Sievenpiper, H.-P. Hsu, J. Schaffner, G. Tangonan, R. Garcia, and S. Ontivero, "Low-profile, four-sector diversity antenna on high-impedance ground plane," *Electron. Lett.*, vol. 36, no. 16, pp. 1343–1345, 2000.

[97] A. P. Feresidis, G. Goussetis, Wang Shenhong, J. C. Vardaxoglou, "Artificial magnetic conductor surfaces and their application to low-profile high-gain planar antennas," *IEEE Trans. Antennas Propag.*, vol. 53, no. 1, pp. 209–215, Jan. 2005.

[98] Kim Dongho and Yeo Junho,"Low-profile RFID tag antenna using compact AMC substrate for metallic objects," *IEEE Antennas Wireless Propag. Lett.*, vol. 7, pp. 718–720, 2008.

[99] J. M. Baracco, L. Salghetti-Drioli, and P. de Maagt, "AMC low profile wideband reference antenna for GPS and GALILEO systems," *IEEE Trans. Antennas Propag.*, vol. 56, no. 8, pp. 2540–2547, Aug. 2008.

[100] Xin Hao, J. B. West, J. C. Mather, J. P. Doane, J. A. Higgins, H. Kazemi, and M. J. Rosker, "A two-dimensional millimeter wave phase scanned lens utilizing analog electromagnetic crystal (EMXT) waveguide phase shifters," *IEEE Trans. Antennas Propag.*, vol. 53, no. 1, pp. 151–159, Jan. 2005.

[101] D. Chicherin, S. Dudorov, D. Lioubtchenko, V. Ovchinnikov, S. Tretyakov, and A. Räisänen, "MEMS-based high-impedance surfaces for millimeter and submillimeter wave applications," *Microw. Opt. Tech. Lett.*, vol. 48, no. 12, pp. 2570–2573, Dec. 2006.

[102] F.-R. Yang, K.-P. Ma, Y. Qian, and T. Itoh, "A novel TEM waveguide using uniplanar compact photonic-bandgap (UC-PBG) structure," *IEEE Trans. Microwave Theory Tech.*, vol. 47, no. 11, pp. 2092–2098, Nov. 1999.

[103] J. A. Higgins, M. Kim, J. B. Hacker, and D. Sievenpiper, "The application of photonic crystals to quasi-optic amplifiers," *IEEE Trans. Microwave Theory Tech.*, vol. 47, no. 11, pp. 2139–2143, Nov. 1999.

[104] A. Cucini, M. Caiazzo, P. Bennati, and S. Maci, "Quasi-TEM waveguides realized by FSS-walls," *IEEE Antennas and Propagation Society International Symposium, 2004.* vol. 1, 20-25 June 2004, pp. 807–810.

[105] D. M. Pozar, S. D. Targonski, and H. D. Syrigos, "Desing of millimeter wave microstrip reflectarrays," *IEEE Trans. Antennas Propag.*, vol. 45, no. 2, pp. 287–296, Feb. 1997.

[106] D. F. Sievenpiper, J. H. Schaffner, H. J. Song, R. Y. Loo, and G. Tangonan, "Two-dimensional beam steering using an electrically tunable impedance surface," *IEEE Trans. Antennas Propag.*, vol. 51, no. 10, pp. 2713–2722, Oct. 2003.

[107] S. Lim, C. Caloz, and T. Itoh, "Metamaterial-based electronically controlled transmission-line structure as a novel leaky-wave antenna with tunable radiation angle and beamwidth," *IEEE Trans. Microwave Theory Tech.*, vol. 52, no. 12, pp. 2678–2690, 2004.

[108] G. T. Ruck, *Radar Cross Section Handbook*, New York: Plenum, 1970.

[109] W. W. Salisbury, Absorbent body of electromagnetic waves, United States Patent 2,599,944, June 10, 1952.

[110] E. F. Knott, J. F. Shaeffer, M. T. Tuley, *Radar Cross Section*, Artech House London, 1993.

[111] J. Reinert, J. Psilopoulos, J. Grubert, and A. F. Jacob, "On the potential of graded-chiral Dallenbach absorbers," *Microw. Opt. Technol. Lett.*, vol. 30, no. 4, pp. 254–257, 2001.

[112] A. R. Chandran, T. Mathew, C. K. Aanandan, P. Mohanan, and K. Vasudevan, "Frequency tunable metallo-dielectric structure for backscattering reduction," *Electron. Lett.*, vol. 40, no. 20, pp. 1245–1246, 2004.

[113] F. Terracher, G. Berginc, "A broadband dielectric microwave absorber with periodic metallizations," *J. of Electromagn. Waves and Appl.*, vol. 13, pp. 1725–1741, 1999.

[114] N. Engheta, "Thin absorbing screens using metamaterial surfaces," in *2002 IEEE International Symposium on Antennas and Propagation*, San Antonio, TX, vol. 2, pp. 392-395, 2002.

[115] D. J. Kern and D. H. Werner, "A genetic algorithm approach to the design of ultra-thin electromagnetic bandgap absorbers," *Microw. Opt. Tech. Lett.*, vol. 38, no. 1, pp. 61–64, 2003.

[116] S. Simms and V. Fusco, "Thin absorber using artificial magnetic ground plane," *Electron. Lett.*, vol. 41, no. 24, pp. 1311–1313, 2005.

[117] H. Mosallaei and K. Sarabandi, "A one-layer ultra-thin meta-surface absorber," *2005 IEEE International Symposium on Antennas and Propagation*, Washington DC, USA, July 2005.

[118] Q. Gao, Y. Yin, D.-B. Yan, and N.-C. Yuan, "A novel radar-absorbing-material based on EBG structure," *Microw. Opt. Tech. Lett.*, vol. 47, no. 3, pp. 228–230, 2005.

[119] S. Simms and V. Fusco, "Tunable thin radar absorber using artifical magnetic ground plane with variable backplane," *Electron. Lett.*, vol. 42, no. 21, pp. 1197–1198, 2006.

[120] S. A. Tretyakov and S. I. Maslovski, "Thin absorbing structure for all incident angles based on the use of a high-impedance surface," *Microw. Opt. Tech. Lett.*, vol. 38, no. 3, pp. 175–178, 2003.

[121] H. Tao, N. I. Landy, C. M. Bingham, X. Zhang, R. D. Averitt, and W. J. Padilla, "A metamaterial absorber for the terahertz regime: design, fabrication and characterization," *Optics Express*, vol. 16, no. 10, pp. 7181–7188, 2008.

[122] N. I. Landy, S. Sajuyigbe, J. J. Mock, D. R. Smith, and W. J. Padilla, "Perfect Metamaterial Absorber," *Physical Review Letters*, vol. 100, p. 207402, 2008.

[123] The homepage of CST corporation, http://www.cst.com/.

[124] H. M. Barlow, "Screened surface waves and some possible applications," (paper 4682 E), *Proc. Inst. Elec. Eng.*, vol. 112, March 1965, pp. 477–482.

[125] J. R. Wait, "On the theory of shielded surface waves," *IEEE Trans. Microwave Theory Tech.*, vol. MTT-15, pp. 410–414, July 1967.

[126] H. M. Barlow, "New features of wave propagation not subject to cutoff between two parallel guiding surfaces," (paper 5227) *Proc. Inst. Elec. Eng.*, vol. 114, Apr. 1967, pp. 421–427.

[127] H. M. Barlow and M. Sen, "Experimental investigation of the hybrid TEM-dual surface wave," *Electron. Lett.*, vol. 3, pp. 450–451, Oct. 1967.

[128] R. Dybdal, L. Peters, and W. Peake, "Rectangular waveguides with impedance walls," *IEEE Trans. Microwave Theory Tech.*, vol. MTT-19, pp. 2–9, Jan. 1971.

[129] H. C. Minnet and B. MacA. Thomas, "A method of synthesizing radiation patterns with axiaf symmetry," *IEEE Trans. Antennas Propagat.*, vol. AP-14, pp. 654–656, Sept. 1966.

[130] V. H. Rumsey, "Horn antennas with uniform power patterns around their axes," *IEEE Trans. Antennas Propagat.*, vol. AP-14, pp. 656–658, Sept. 1966.

[131] E. Lier and P.-S. Kildal, "Soft and hard horn antennas," *IEEE Trans. Antennas Propag.*, vol. 36, no. 8, pp. 1152–1157, 1988.

[132] S. P. Skobelev and P.-S. Kildal, "Analysis of conical quasi-TEM horn with a hard corrugated section," *IEEE Trans. Antennas Propag.*, vol. 51, no. 10, pp. 2723–2731, 2003.

[133] M. Thumm, "Computer-aided analysis and design of corrugated TE_{11} to HE_{11} mode converters in highly overmoded waveguides," *Int. J. Infrared Millimeter Waves*, vol. 6, no. 7, pp. 577–597, 1985.

[134] H. Xin, J. B. West, J. C. Mather, J. P. Doane, J. A. Higgins, H. Kazemi, and M. J. Rosker, "A two-dimensional millimeter wave phase scanned lens utilizing analog electromagnetic crystal (EMXT) waveguide phase shifters," *IEEE Trans. Antennas Propag.*, vol. 53, no. 1, pp, 151–159, Jan. 2005.

[135] H. Xin, A. Higgins, J. Hacker, M. Kim, and M. Rosker, "Electromagnetic crystal (EMXT) waveguide band-stopp filter," *IEEE Microwave Compon. Lett.*, vol. 13, no. 3, pp. 108–110, 2003.

[136] A. Higgins, H. Xin, and A. Sailer, "Tunable millimeter wave band pass filter using electromagnetic crystal sidewalls," in *2004 IEEE MTT-S Int. Microwave Symp. Dig.*, June 2004, pp. 1295–1298.

[137] M. N. M. Kehn, M. Nannetti, A. Cucini, S. Maci, and P.-S. Kildal, "Analysis of dispersion in dipole-FSS loaded hard rectangular waveguide," *IEEE Trans. Antennas Propag.*, vol. 54, no. 8, pp. 2275–2282, Aug. 2006.

[138] C. L. Holloway, E. F. Kuester, and D. Novotny, "Waveguides composed of metafilm/metasurfaces: the two-dimensional equivalent of Metamaterials," *IEEE Antennas Wireless Propag. Lett.*, vol. 8, pp. 525–529, 2009.

[139] W. Rotman, "A study of single surface corrugated guides," *Proc. I.R.E.*, vol. 39, pp. 952–959, Aug. 1951.

[140] R. S. Elliott, "On the theory of corrugated plane surfaces," *IRE Trans. Antennas Propagat.*, pp. 71–81, Apr. 1954.

[141] R. A. Hurd, "The propagation of an electromagnetic wave along an infinite corrugated surface," *Can. J. Phys.*, vol. 32, pp. 727–734, 1954.

[142] L. A. Vainshtein, "Propagation of electromagnetic waves on a corrugated surface," *Soviet Phys.-Tech. Phys. 1*, p. 379, 1956.

[143] J. Ehrlich and L. L. Newkirk, "Corrugated surface antennas," in *Proc. IRE Nat. Conv. Rec.*, pp. 18–33, March 1953.

[144] R. W. Houghardy and R. C. Hansen, "Scanning surface wave antennas – oblique surface waves over corrugated conductor," *IRE Trans. Antennas Propagat.*, vol. 6, pp. 370–376, Oct. 1958.

[145] L. O. Goldstone and A. A. Oliner, "A note on surface waves along corrugated structures," *IRE Trans. Antennas Propagat.*, vol. 7, pp. 62–73, July 1959.

[146] V. H. Rumsey, *Electromagnetic Theory and Antennas*, (Ed. E. C. Jordan), New York: Macmillan, 1963.

[147] P.-S. Kildal, A. A. Kishk, and A. Tengs, "Reduction of forward scattering from cylindrical objects using hard surfaces," *IEEE Trans. Antennas Propagat.*, vol. 44, pp. 1509–1520, Nov. 1996.

[148] Z. Ying, P.-S. Kildal, and A. A. Kishk, "Study of different realizations and calculation models for soft surfacees by using a vertical monopole on a soft disk as a test bed," *IEEE Trans. Antennas Propagat.*, vol. 44, pp. 1474–1481, Nov. 1996.

[149] E. Brown, C. Parker, and E. Yablonovitch, "Radiation properties of a planar antenna on a photonic-crystal substrate," *J. Opt. Soc. Amer. B, Opt. Phys.*, vol. 10, pp. 404–410, 1993.

[150] S. Cheng, R. Biswas, E. Ozbay, S. McCalmont, G. Tuttle, and K.-M. Ho, "Optimized dipole antennas on photonic band gap crystals," *Appl. Phys. Lett.*, vol. 67, pp. 3399–3402, 1995.

[151] E. Brown and O. McMahon, "High zenithal directivity from a dipole antenna on a photonic crystal," *Appl. Phys. Lett.*, vol. 68, pp. 1300–1303, 1996.

[152] M. Kesler, J. Maloney, B. Shirley, and G. Smith, "Antenna design with the use of photonic band-gap materials as all-dielectric planar reflectors," *Microw. Opt. Technol. Lett.*, vol. 11, pp. 169–174, 1996.

[153] M. Sigalas, R. Biswas, Q. Li, D. Crouch, W. Leung, R. Jacobs-Woodbury, B. Lough, S. Nielsen, S. McCalmont, G. Tuttle, and K.-M. Ho, "Dipole antennas on photonic band-gap crystals: Experiment and simulation," *Microw. Opt. Technol. Lett.*, vol. 15, pp. 153–156, 1997.

[154] T. Rozzi and M. Mongiardo, *Open Electromagnetic Waveguides*, Inst. Elect. Eng. Electromagnetic Waves Series 47. London, U.K, 1997.

[155] P. Baccarelli, P. Burghignoli, F. Frezza, A. Galli, P. Lampariello, G. Lovat, and S. Paulotto, "Fundamental modal properties of surface waves on metamaterial grounded slabs," *IEEE Trans. Microwave Theory Tech.*, vol. 53, no. 4, pp. 1431–1442, April 2005.

[156] E. Arvas and R. F. Harrington, "Computation of the magnetic polarizability of conducting disks and the electric polarizability of apertures," *IEEE Trans. Antennas Propagat.*, vol. AP-31, no. 5, pp. 719-725, Sept. 1983.